ELSEVIER

Contents lists available at ScienceDirect

Ore Geology Reviews

journal homepage: www.elsevier.com/locate/oregeorev



Integrated O, Fe, and Ti isotopic analysis elucidates multiple metal and Luid sources Lor magnetite Loron the Ernest Henry Iron oxide copper gold (IOCG) Deposit, Queensland, Australia

Christopher Emproto a,*, Ryan Mathur b, Adam Simon a, Ilya Bindeman c, Linda God □rey d, Courteney Dhnaram e, Vladimir Lisitsin e

- a University of Michigan, Ann Arbor, MI, USA
- $^{\mathrm{b}}$ Juniata College, Huntingdon, PA, USA
- ^c University of Oregon, Eugene, OR, USA
- d Rutgers University, New Brunswick, NJ, USA
- e Geological Survey of Queensland, City East, Queensland, Australia

ARTICLEINFO

Keywords: IOCG Ernest Henry O isotopes Fe isotopes Ti isotopes

ABSTRACT

Iron oxide copper gold (IOCG) deposits are globally important sources o□Cu; however, their origins remain poorly understood with respect to the metal and □uid sources involved in their □ormation. In this work, we utilize integrated Fe, Ti, and O isotopic data□or magnetite to trace major metal and uid inputs□or the Proterozoic-aged Ernest Henry IOCG deposit—the largest known IOCG deposit in the Cloncurry District, Queensland, Australia. Magnetite separates □rom ore stage and pre-ore biotite-magnetite (bt-mgt) and magnetite-actinolite (mgt-act) alteration assemblages□rom Ernest Henry were analyzed□or their O, Fe, and Ti isotope abundances, reported as $\delta^{18}O$ (VSMOW), $\delta^{56}Fe$ (IRMM-14), and $\delta^{49}Ti$ (OL-Ti). Select magnetite samples were also analyzed \Box or (reported asΔ' ¹⁷O_{0.5305}) and range□rom□0.118 to□0.056‰—suggesting evaporitic input. Theδ □rom ore stage (+1.57 to+7.36‰), bt-mgt (+0.34 to+5.68‰), and mgt-act (+1.68 to+2.10‰) samples are consistent with a magmatic-hydrothermal origin or ore and pre-ore mineralizing uids at Ernest Henry; non $magmatic \delta$ 18O values>c. 5% may be explained through localized carbonate wall rock assimilation. Despite this, δ ⁵⁶Fe values \Box or ore stage (\Box 0.50 to +0.33%), bt-mgt (\Box 0.65 to +0.38%), and mgt-act (\Box 0.26 to +0.30%) magnetite are generally isotopically lighter than the accepted range (c.+0.06 to+0.49%) or igneous and magmatic-hydrothermal magnetite and exhibit a relatively large range o□c. 1‰, suggesting Fe source mixing within the deposit. Ore stage magnetite δ ⁴⁹Ti (\Box 1.64 to +3.79‰; avg: +1.49‰; 2 σ =2.63‰) compositions are generally higher and more variable than either the bt-mgt (-0.44 to+1.49%; avg:+0.62%; 2 $\sigma = 1.13\%$) or mgt-act (+0.27 to +1.89%; avg: +1.05%; 2 $\sigma = 1.56\%$) and suggest that Ti isotope \Box ractionation occurred due to di□□erential mobility in the□uid. The data are best explained by models invoking both magmatic and nonmagmatic metal and □uid input. Fluid □ow channeled between the □ootwall and hanging wall shear zones introduced non-magmatic Fe that may have been leached or molecal mafe units by magmatic-hydrothermal □uids, resulting in neo□ormed and regeneratively replaced magnetite with magmaticδ ¹⁸O, but non-magmatic δ⁵6Fe values during pre-ore alteration. These□uids may have mixed with Fe-poor evaporitic□uids prior to magnetite ormation. Later magmatic Fe and O contributions during ore stage mineralization resulted in magnetite with variableδ ⁵⁶Fe and irresolvableδ ¹⁸O overprinting. Ernest Henry is the frst known example o□an IOCG deposit with a major leached metal component identifed through metal stable isotope geochemistry.

1. Introduction

Sustainable supplies onelements including Fe, Cu, rare earth

elements (REE), and other metals are required to build and maintain renewable energy in \Box astructure. The demand \Box or Cu alone is expected to increase by as much as 350 % by 2050 and finding new sources o \Box Cu is

E-mail address: cemproto@umich.edu (C. Emproto).

^{*} Corresponding author.

paramount to closing a potential supply and demand gap (Elshkaki et al., 2016). The Iron Oxide Copper Gold (IOCG) class o mineral deposits is an increasingly significant source o□Cu and has strong exploration potential as new geochemical vectoring tools are developed and the origin o these deposits becomes clearer (Hitzman et al., 1992; Sillitoe, 2003; Barton, 2014). Deposits sharing the physical and geochemical characteristics o□the IOCG class may be broadly described as hydrothermal, structurally controlled Fe oxide (±Cu sulfde) mineralization enveloped by extensive Na-Ca-K alteration haloes and exhibiting characteristic elemental enrichment suites comprising Fe oxides (including magnetite and/or hematite), Cu, Au, Ag, REE, P, U, and Co (Hitzman et al., 1992; Sillitoe, 2003; Barton, 2014). Some workers consider iron oxide apatite (IOA)—or "Kiruna type"—deposits to be a subset within the IOCG clan, whereas others propose that IOA systems represent the deeper, hotter roots o <u>HOCG</u> deposits or that IOCG deposits <u>arm</u> <u>room</u> the overprinting o□IOA deposits by Cu-rich□uids (Barton, 2014; Simon et al., 2018; Rodriguez-Musta □a et al., 2020; del Real et al., 2021). Analogues in the Cretaceous Chilean Iron Belt suggest that IOCG deposits can□orm in continental arc environments associated with subduction zone magmatism; however, other tectonic environments are believed to be represented in the global IOCG suite—hinting that there may be multiple geologic pathways to IOCG-style mineralization and potentially inhibiting a"mineral systems" approach (Barton, 2014; Rodriguez-Musta □a et al., 2020; Groves et al., 2022).

While the Cu-Au mineralization in IOCG systems is generally agreed upon to be hydrothermal, no consensus exists regarding the source(s) o□ their contained metals and their mobilizing uids (Barton, 2014). This work utilizes a novel isotopic approach to test proposed IOCG rmation models using spatially receremed samples o magnetite mom the Proterozoic Ernest Henry deposit in the Cloncurry District, Queensland, Australia. The source o□ore□uids□or the Cloncurry IOCG deposits remains the topic o□extensive debate and at least□our broadly defned □uid sources are proposed □or these systems including magmatichydrothermal □uids, basinal brines, and combinations o □these with sedimentary pore □uids and metamorphic □uids (Barton and Johnson, 1996; Baker et al., 2001, 2008; Cave et al., 2018; Fisher and Kendrick, 2008; Schlegel et al., 2017, 2018). In the magmatic-hydrothermal model, the □uids and metals are sourced □rom an evolving silicate magma in the shallow crust (Hitzman et al., 1992; Sillitoe, 2003; Chiaradia et al., 2006; Pollard, 2006; Schlegel et al., 2017; Simon et al., 2018). The uids in the basinal brine model comprise hypersaline connate □uids that scavenge metals □rom the shallow crust; a nearby intrusion provides heat to drive the convection o□these□uids (Oreskes and Einaudi, 1992; Haynes et al., 1995; Barton and Johnson, 1996; Bastrakov et al., 2007; Xavier et al., 2008). Fluids in the sedimentary pore □uid model consist o □ sedimentary pore water potentially mixed with metamorphic-derived uids (Fisher and Kendrick, 2008; Schlegel et al., 2018). The metamorphic uid model proposes that devolatilization during regional prograde metamorphism o□the local volcanic and sedimentary stratigraphy resulted in rock-bu [@red brines (Benavides et al., 2007; Kendrick et al., 2007; Fisher and Kendrick, 2008). Some models propose multiple □uid sources □or precipitating Fe and Cu-Au mineralization with or without uid mixing as the mineralization trigger (Baker et al., 2008; Fisher and Kendrick, 2008; Cave et al., 2018).

Hypothesized □id compositions □r Cloncurry IOCG deposits span □rom hot and hypersaline brines to cooler and less saline Cu+U-rich aqueous solutions (Williams et al., 2001; Baker et al., 2008; Torresi et al., 2012; Schlegel et al., 2018). A prevailing hypothesis□or the ore □uid chemistry proposes that Cu-Au mineralization derived□rom the infltration o□lypersaline, NaCl- and CO 2-rich brines with relatively low (<c. 200 ppm) Cu concentrations at pressures o□c. 1.3–3.7 kbar (Baker et al., 2008; Rusk et al., 2010). Although low (c. 150 ppm) Cu concentrations are consistent with hypotheses suggesting a crustally-derived □uid, in situ analyses have measured Cu concentrations o□c. 3000 ppm in some□uid inclusions interpreted to be coeval with Cu-Au mineralization in Cloncurry IOCG deposits and may alternatively

suggest that Cu-poor □id inclusions could simply be pre-mineralization □uid or post-mineralization "spent" □uid (Baker et al., 2008; Rusk et al., 2010; Schlegel et al., 2021). A clear understanding o□the□uids is clouded by the presence o□multiple di□□erent types o□□id inclusions including those with magmatic-hydrothermal and evaporitic signatures, respectively (Baker et al., 2008). The heterogeneous□uid compositions and provenance signatures within individual deposits have spurred some to hypothesize□uid mixing as an important process in IOCG□ormation (Fisher and Kendrick, 2008; Baker et al., 2008).

Here we present O, Fe, and Ti stable isotope data or magnetite or mag the world-class Ernest Henry IOCG deposit and integrate our data with existing spatial datasets rom the deposit to evaluate existing models explaining the mineralization history and the source o□successive□uid generations at Ernest Henry. Recently, Fe and O stable isotope pairs have been important evidence in in Terring magmatic metal and Tuid sources □or magnetite□rom IOA and IOCG deposits (Bilenker et al., 2016; Childress et al., 2016, 2020a, b; Troll et al., 2019; Rodriguez-Musta □a et al., 2020, 2022). While O isotope compositions are sensitive to secondary alteration □rom hydrothermal and supergene □uids, Fe isotopic compositions are considered more stead ast under such conditions and are considered as a more reliable indicator o□metal provenance (Bilenker et al., 2016; Troll et al., 2019). Like Fe, Ti isotope signatures are also thought to resist hydrothermal and metamorphic overprinting due to the low solubility o□Ti and common Ti-bearing minerals in most □ids. In presenting the frst published Ti isotope measurements □rom a mineralized system, we demonstrate that the above assumption is □awed, providing insight into Ti isotope□ractionation in ligand-rich hydrothermal systems and opening the door□or Ti isotopes as a vectoring method. The stable isotope data presented herein provide the opportunity to trace metal and □uid sources, □uid mixing, and the assimilation o host rock components via 3D spatial analysis to develop a clearer picture regarding the metallogeny and mineralization history o the Ernest Henry IOCG deposit.

2. Geologic background

The Ernest Henry deposit is a blind IOCG-style Cu-Au deposit hosted in southeast-dipping, sheared Proterozoic metavolcanic rocks o the Eastern Succession o□the Mount Isa Inlier, northwest Queensland, Australia (Fig. 1) (Twyerould, 1997; Ryan, 1998; Austin et al., 2021b). The Cloncurry District in the Eastern Succession hosts a series o GOCG deposits including Starra and Mount Elliott, however, Ernest Henry is the largest known IOCG deposit in the district and the second largest IOCG deposit in Australia (□ollowing Olympic Dam) with an initial resource estimate o□167 Mt o□ore grading 1.1 % Cu and 0.54 g/t Au (Lilly et al., 2017; Ryan, 1998; Hutton et al., 2012). First discovered in 1991 through drilling o \square a magnetic anomaly target, the deposit has been operated commercially since 1998 (Webb and Rowston, 1995; Ryan, 1998; Schlegel et al., 2021). Economic Cu-Au mineralization at Ernest Henry occurs in a south-plunging pipe-like structure located between two southeast-dipping shear zones: the dotwall shear zone in the northwest and the hanging wall shear zone in the southeast (Webb and Rowston, 1995; Austin et al., 2021a, b). The Eastern Succession consists o Molcanic and metamorphosed volcanic, evaporite, and carbonate units that were episodically deposited into an intracontinental ri□t basin between c. 1890-1610 Ma (Blake, 1987; Blake and Stewart, 1992; Foster and Austin, 2008). The metamorphosed volcanic suite hosting IOCG mineralization at Ernest Henry consists o a series o andesitic to dacitic lavas with minor basaltic units erupted as the temporal and petrologic equivalents o□the c. 1745 Ma Mount Fort Constantine metavolcanic suite (Page and Sun, 1998). These rocks were later de Grmed during the Isan Orogeny, with peak metamorphic conditions attaining greenschist to amphibolite □acies and undergoing regional sodic(-calcic) alteration due to structurally-channeled 400-500 °C brines during E-W shortening at c. 1585 Ma (de Jong and Williams, 1995). Economic Cu-Au mineralization at Ernest Henry likely occurred at c. 1530 Ma associated with

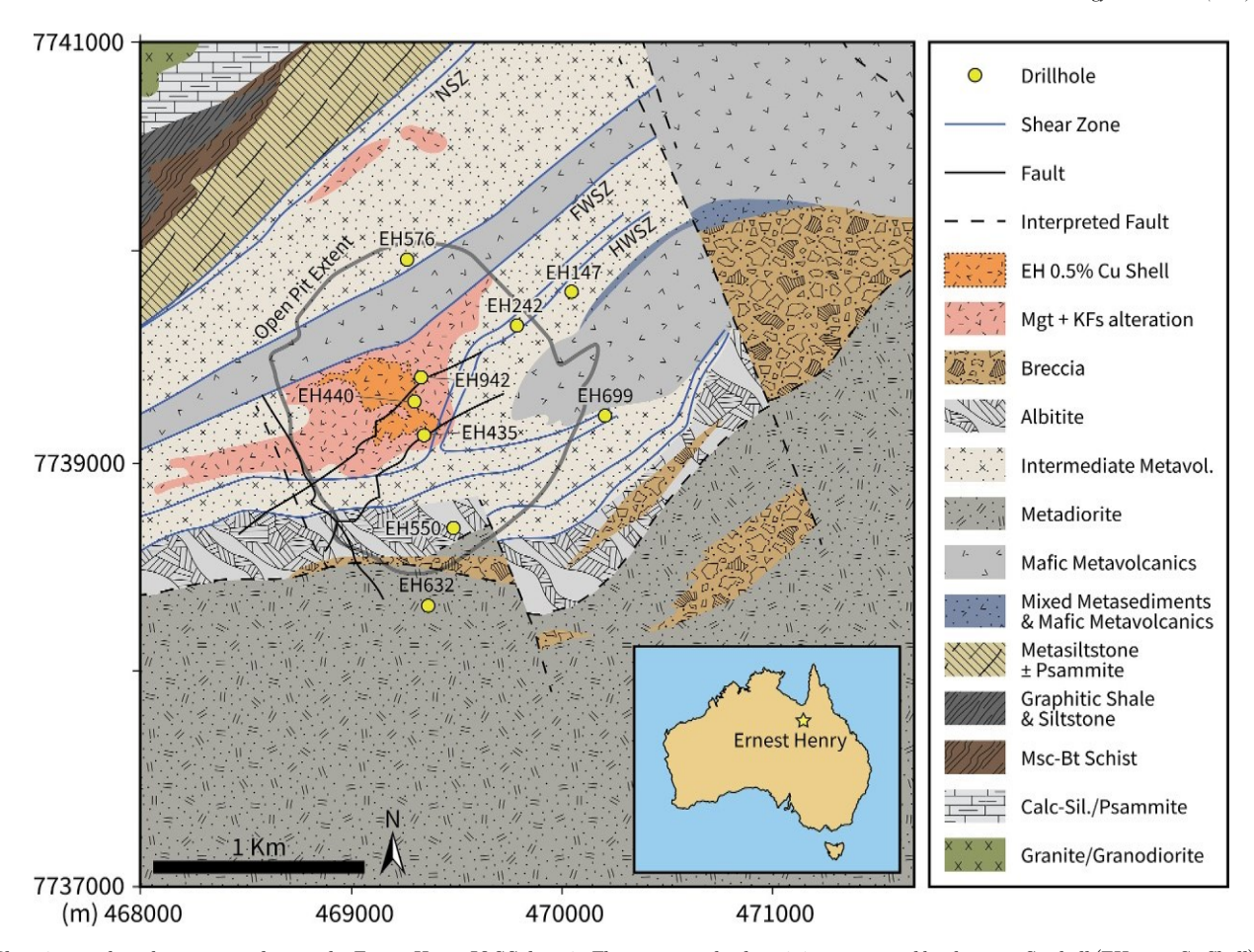


Fig. 1.Plan view o□the subsur□ace geology o□the Ernest Henry IOCG deposit. The extent o□the deposit is represented by the 0.5% Cu shell (EH 0.5% Cu Shell). Modifed a□ter O'Brien (2016). FWSZ: Footwall shear zone; HWSZ: Hanging wall shear zone; NSZ: North shear zone.

the intrusion $o\square A$ -type granitoids $o\square$ the Williams-Naraku suite in the Mount Isa Inlier (Ryan, 1998; Belousova et al., 2001; Mark et al., 2006b; Cave et al., 2018).

Magnetite at Ernest Henry occurs within several mineralogically distinct assemblages including biotite-magnetite (bt-mgt), magnetiteactinolite (mgt-act), and ore stage assemblages. Bt-mgt, K-Mn-Fe, and mgt-act alteration directly preceded ore mineralization, as the reported U-Pb titanite age interpreted to represent bt-mgt alteration (1514+11/-8 Ma) is nearly within error o□the interpreted age o□regional A-type granitic magmatism (c. 1530 Ma) in □erred to be the source o □ Cu in the district (Mark et al., 2006b). Biotite-magnetite alteration was subsequently overprinted by K-Mn-Fe alteration consisting on additional biotite and magnetite alongside K□eldspar, carbonates, and minor garnet (Schlegel et al., 2018). The timing o ingt-act alteration is unclear, but veins o□magnetite-actinolite appear to cross-cut areas o□bt-mgt mineralization in deeper portions o□the orebody (Ernest Henry Mining, personal communication 2022). Minor chalcopyrite occurs within the mgt-act mineralization, which may indicate that mgt-act alteration represents early Cu mineralization at Ernest Henry (Mark et al., 2006b; Schlegel et al., 2021). During later ore stage mineralization, magnetite Grmed alongside K eldspar, chalcopyrite, pyrite, and native Au (Mark et al., 2006b; Schlegel et al., 2021). The ore zone was then variably overprinted by later carbonate veining and post-mineralization alteration (Schlegel et al., 2021).

At shallower levels o the Ernest Henry deposit, mineralization is primarily present as infll between rounded clasts o totassically altered metavolcanic host rocks, whereas at depth, both infll and partial replacement o clasts are present (Rusk et al., 2010). Previous interpretations o the mineralized breccia at Ernest Henry involved an

explosive-implosive eruptive model or ore mineralization caused by □uid over pressurization due to the mixing o□magmatic-hydrothermal uid with basinal brine, inspiring a diatreme-like structural interpretation o□the deposit (Oliver et al., 2006; Mark et al., 2006a; Rusk et al., 2010; Cave et al., 2018). The hypothesis that brecciation was synchronous with Fe and Cu-Au mineralization was supported by the occurrence o rounded clasts o pyrite, chalcopyrite, and magnetite within the lower levels o the breccia as well as the partial replacement o clasts within it (Rusk et al., 2010). More recent interpretations instead avor brecciation due to □uid-driven □ailure under generally ductile conditions during regional metamorphism o \Box the Mount Isa Inlier prior to c. 1530 Ma Cu-Au mineralization collowed by post-mineralization brittle de cormation (Marshall and Oliver, 2008; Cave et al., 2018; Austin et al., 2021a, b). Despite intense cross-disciplinary scrutiny since shortly a ter its discovery, understanding on the mineralization history at Ernest Henry enjoys no broad consensus and continues to evolve to reconcile geochronological, geochemical, and petrographic data (Baker et al., 2008; Cave et al., 2018; Austin et al., 2021a, b; Schlegel et al., 2021, 2022).

3. Methods

Core and rock chip samples \Box rom the Ernest Henry deposit were provided by the Geological Survey $o\Box$ Queensland (GSQ) \Box or analysis. Samples were sourced \Box om a series $o\Box$ drill cores traversing di \Box \Box rent sections $o\Box$ the ore deposit and comprise a representative suite $o\Box$ lithologies \Box rom the Ernest Henry ore stage, bt-mgt, and mgt-act alteration assemblages \Box ound throughout and adjacent to the deposit. Drill cores EH576 and EH942 intersect the nearby Erebus prospect c. 1 km NNW $c\Box$

the Ernest Henry orebody (c. 550 m depth) and exhibit mgt-act and bt-mgt alteration interpreted as related to equivalent alteration occurring closer to the orebody. Ore stage magnetite samples are interpreted to be petrogenetically related to economic Cu-Au mineralization (Schlegel et al., 2021; this study). More detailed petrography data \Box or most samples included in this work are presented in Schlegel et al. (2021); see Appendix Table S1 \Box or additional sample in \Box ormation. Magnetite textures and mineral associations were assessed on polished samples using scanning electron microscopy backscattered electron imaging (SEM-BSE) methods at the Electron Microbeam Analysis Lab (EMAL) at the University o \Box Michigan using a JEOL JSM-7800FLV feld emission scanning electron microscope.

Stable isotope data were obtained from magnetite mineral separates prepared through magnetic separation o crushed rock samples. Due to the small (<c. 100 µm) average grain size o magnetite in most samples, magnetite separates were obtained through a series o□magnetic separations without hand picking. Magnetic separates were successively reduced to powder using a pestle and mortar over several crushing steps between each additional magnetic separation to remove impurities liberated during crushing and obtain the purest possible magnetite □ractions. Magnetite separates rather than whole rock powders were utilized □or analysis due to the highly heterogeneous nature o □ore mineralization observed at Ernest Henry. The Ti budget at Ernest Henry is likely significantly impacted by biotite, with a lesser in □uence □rom ilmenite, rutile, and titanite (Schlegel et al., 2021). However, the targeting oaa single mineral phaseaacilitates comparison across the di [rent assemblages ound throughout and near the deposit and ourther enables comparison with magnetite isotope data from the literature. All magnetite sampled □or this study appeared □resh without any obvious signs o□oxidation or sur□ace weathering.

Magnetite O isotope compositions were measured at the University o□Oregon using BrF 5 in a laser□uorination line connected to a Thermo MAT 253 gas isotope ratio mass spectrometer (IRMS) operated in dual inlet mode. Approximately 2 mg o□magnetite mineral separates were used or each analysis. Magnetite samples were pretreated overnight to obtain a clean blank prior to analysis, ensuring that any reactive secondary phases were removed by the BrF₅ pretreatment. The Gore Mountain garnet (GMG) standard (+6.52‰) and UWG-2 garnet (+5.8 ‰) were measured be □ore, during, and □ollowing sample analyses (Loewen and Bindeman, 2016). Long-term monitoring or errors on these standards yields an average 2σ o_ $\pm 0.08 \text{\%} \delta$ $^{18}\text{O}_{\square}\text{or}$ the laboratory and methodology. Yields (µmol/mg o□O 2 gas extracted) were checked using a Baratron gauge; yields □ rδ 18O analyses are presented in Table S2. For triple O analyses, the generated gas was sent through a 9□t gas chromatographic zeolite column with a 5 Å molecular sieve to remove NF_x contaminants and then prozen within the zeolite. A timed 20 min LN2slush accompanied each analysis to urther prevent any contamination. The gas was then run □or 3 to 8 cycles o □8 sample-standard comparison (24 or 64 repetitions; 32□or most samples); standard mass spectrometric errors $\Box r \Delta'$ 17 $O_{0.5305}$ on these were in the vicinity o $\Box 0.01$ %. The San Carlos olivine (SCO) was used as a triple O standard and its values were □0.051±0.01‰, in agreement with Miller et al. (2020). Normalization $o\Box\Delta'$ ¹⁷O to this was 0.01‰and δ ¹⁸O $o\Box$ SCO during the $\Delta^{'17}$ O sessions was in 4.9-5.5% range.

Sample dissolution and column chemical separation□or Fe and Ti isotope analyses were carried out at Juniata College□ollowing the methodology o ■Mathur et al. (2022). A total o □cl 50 mg o □magnetite □mom each sample were dissolved in a 4 ml solution o □25 % 15.2 M HNO 3 and 75 % 10 M HCl over a hot plate. Separate solutions□or Fe and Ti isotopes were obtained through a two-step purification process using Bio-Rad AG MP-1 (HCl□orm, 100–200 mesh) and prepacked Eichrom TODGA anion exchange resins. During the first step, Fe is separated □mom the sample solution and retained on the Bio-Rad AG MP-1 column resin using procedures identical to that o□ Mar´echal et al. (1999) and Mathur et al. (2005); Fe is retrieved□rom the resin using a 2 M HCl elution step. During the second column step, the sample solution is loaded onto a

prepacked TODGA column and rinsed with ultrapure water and HNO $_3$ prior to Ti elution using HNO $_3$ and 1 % hydrogen peroxide. Isobaric element abundances and yields \square rom the chromatography were monitored to ensure negligible concentrations and>91 % yields using inductively coupled plasma optical emission spectrometry (ICP-OES) via an Agilent 5900 ICP-OES instrument at Juniata College. All concentrations were calculated with calibration curves between 0.5 and 20 ppm with values corrected using Y as an internal standard.

Isotope sample solutions were analyzed using multi-collector inductively coupled mass spectrometry (MC-ICP-MS) Neptune MC-ICP-MS at Rutgers University and Washington State University. Titanium was measured on both instruments and \Box rther descriptions o \Box the process and instrument parameters are provided in Mathur et al. (2022). The instrumentation setup \Box or Ti was identical to that o \Box Zhu et al. (2002) and mass bias was corrected \Box or by standard sample bracketing. The bracketing Ti isotope standard used \Box or this study was graciously donated by N. Dauphas at the University o \Box Chicago (Greber et al., 2021; Zhang et al., 2011). The 2 σ error \Box or the Ti isotope analyses was determined to be \pm 0.14%via multiple, \Box ull procedural measurements o \Box a solid synthetic Fe-Ti oxide standard.

The Fe isotope solutions were measured at Washington State University with instrumentation setup and data reduction identical to Yesavage et al. (2016). Iron isotope samples were measured in duplicate, and the reported value is an average o \Box the two measurements. The 2 σ □or each sample is lower than the reported error below. The NIST SRM 3126a Fe isotope standard was monitored throughout the analytical session and produced a δ ⁵⁶Fe= +0.29±0.07‰(2 σ ; N=14) which is within the error oppreviously reported values. Given this sample was measured the most throughout the measuring sessions, the error \square or all samples is assumed to be±0.07‰. Several previously measured magnetite values reported in the literature were replicated to □urther assess the reproducibility on the technique; these data are presented in Appendix Table S3. Most samples were reproduced within or nearly within error, although sample heterogeneity may explain additional minor discrepancies (Knipping et al., 2019). The largest di□□erence between our replicate and the published value was+0.16% or sample LC-05-82.6 where our measuredδ ⁵⁶Fe value was □0.08‰whereas Bilenker et al. (2016) report a δ ⁵⁶Fe value o \Box +0.08 \pm 0.03‰; Knipping et al. (2019) analyzed this sample using in situ laser ablation techniques and observed heterogeneity outside o the analytical error with respect to the core and rim (Table S3).

4. Results

Representative SEM-BSE images o magnetite are presented in Fig. 2. Several styles o magnetite were observed during SEM-BSE imaging. In most samples, magnetite is closely associated with titanite and Mn-rich ilmenite (Fig. 2). Magnetite generally contains—ew inclusions, although some samples host abundant inclusions o Laddspar or albite (Fig. 2b, c). Minor inclusion phases include chalcopyrite, Mn-rich ilmenite, pyrite, and titanite. Magnetite is commonly associated with titanite and ilmenite and may be rimmed by titanite. Quartz occurs as—racture filings and along grain boundaries in magnetite clusters. No major element zoning in magnetite was observed using SEM X-ray energy dispersive spectroscopy (XEDS) mapping and SEM-BSE imaging.

Magnetite sample in□ormation and $\delta^{18}O, \delta^{56}Fe$, and $\delta^{49}Ti$ data are presented in Table 1; triple O isotope data are presented in Table 2. Magnetite stable isotope compositions are reported and discussed relative to Vienna standard mean ocean water (VSMOW), Standard 14 \Box rom the Institute \Box r Re \Box rence Materials and Measurements (IRMM·14), and the Origins Laboratory Ti (OL-Ti) standard \Box rof $\delta^{18}O/\delta^{17}O, \delta^{56}Fe$, and δ^{49} Ti, respectively. For δ^{56} Fe and δ^{49} Ti data, only data displaying mass dependent \Box ractionation were included.).

The magnetite δ ¹⁸O values range \Box rom +1.57 to +7.36% with an average δ ¹⁸O o \Box +2.97±2.66%(2 σ ; N=21) \Box rore stage magnetite, +0.34 to +5.68% with an average δ ¹⁸O o \Box +2.07±2.52%(2 σ ; N=20)

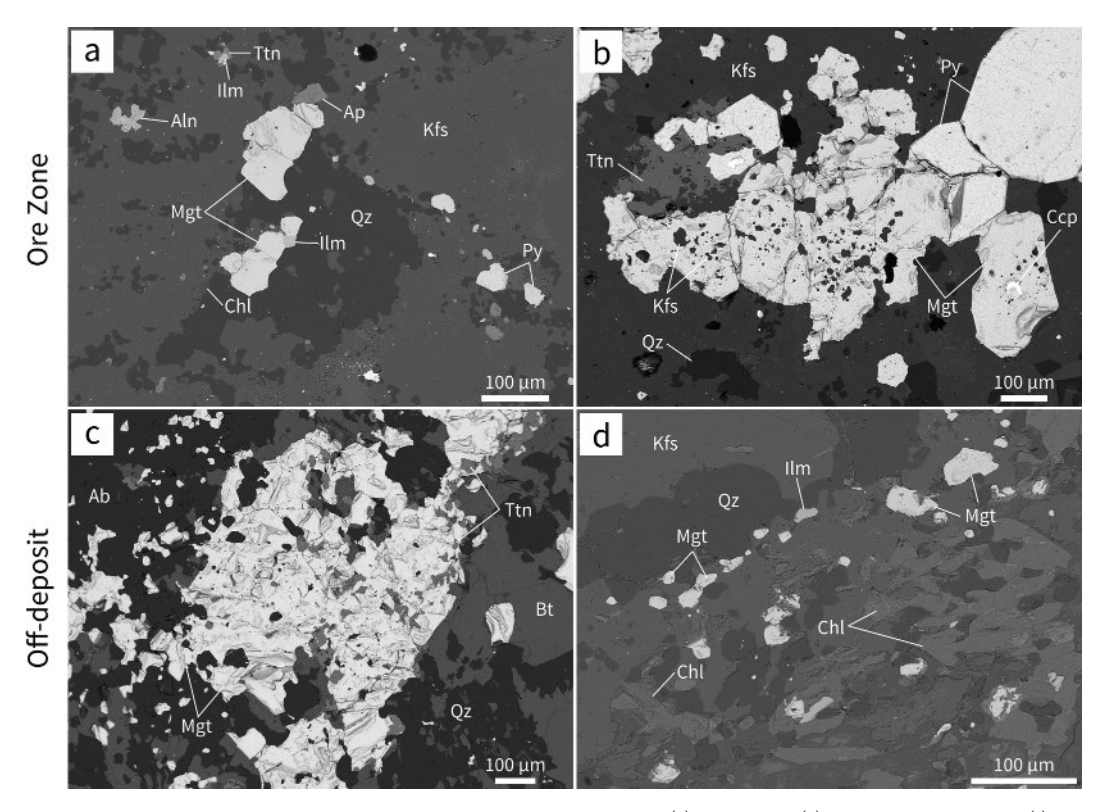


Fig. 2.SEM-BSE images on magnetite and associated minerals from ore stage samples EH191 (a) and EH164 (b), bt-mgt sample EH117 (c) and mgt-act sample MS_EHM213 (d). Ab: albite; Aln: allanite; Ap: apatite; Bt: biotite; Ccp: chalcopyrite; Chl: chlorite; Ilm: ilmenite; Kis: Kis: Kis: Kis: Kis: Kis: Kis: Aln: allanite; Ap: apatite; Bt: biotite; Ccp: chalcopyrite; Chl: chlorite; Ilm: ilmenite; Kis: Kis: Kis: Aln: allanite; Ap: apatite; Ap: apatite; Bt: biotite; Ccp: chalcopyrite; Chl: chlorite; Ilm: ilmenite; Kis: Kis: Aln: allanite; Ap: apatite; Ap

bt-mgt magnetite, and +1.68 to +2.10% with an average δ 18 O o \Box +1.96±0.38‰(2 σ; N=4) mgt-act magnetite. Magnetiteδ ¹⁸O values □ or all samples primarily □all within the range consistent with igneous and magmatic-hydrothermal magnetite (c.+1 to+4.5%) (Taylor, 1967, 1968; Bilenker et al., 2016; Troll et al., 2019). However, two ore stage magnetite samples (EH209:+5.47%; EH211:+7.36%) and one bt-mgt sample (MS_EHM255:+5.675%) exhibit higher δ 18O values than those consistent with a magmatic origin and two bt-mgt samples plot at δ $^{18}{\rm O}$ values lower than the magmatic origin range; all other pre-ore samples exhibitδ ¹8O values consistent with the range □or magmatic magnetite. The δ ¹⁸O range (0.42‰) □ or mgt-act magnetite is remarkably narrow compared to the bt-mgt and ore stage magnetite. The ore stage magnetite samples plotting outside the magmatic origin range are rom the deepest sampled parts on the EH435 drill core—which plunges subvertically through the center o□the orebody; magnetite samples□rom this drill core show monotonically increasing δ ¹⁸O values with depth (Fig. 4). No other drill core shows this monotonic relationship, although the highestδ ¹8O values are generally □ound at depth in the drill cores accessing the ore zone (Fig. 4). Ore stage samples analyzed □or triple oxygen isotopes yielded Δ' ¹⁷O values o \square 0.094 \pm 0.043‰(2 σ ; N=7) and two bt-mgt samples yielded∆' 17O values o□□0.073‰and□0.069 %, respectively Fig. 5).

The magnetite δ ^{56}Fe values range \Box rom $\Box 0.50$ to +0.33% with an average δ ^{56}Fe o \Box $\Box 0.09\pm0.52\%(2$ $\sigma;$ N=8) \Box or ore stage magnetite, $\Box 0.65$ to +0.38% with an average δ

 $\sigma; N=13) \\ \mbox{$\square$ or the bt-mgt magnetite,} \\ \mbox{and} \\ \mbox{\square 0.26 to} + 0.30 \\ \mbox{w with an average δ^{56} Fe o} \\ \mbox{\square \square on mgt-act magnetite.} \\ \mbox{M an average δ^{56} Fe values are generally lower than the range proposed} \\ \mbox{\square or magmatic magnetite (c.+0.06 to} \\ \mbox{t o+0.49 \\ \mbox{\emptyset o$} \\ \mbox{$\delta^{56}$ Fe). Only a} \\ \mbox{\square ew ore stage magnetite samples exhibit δ^{56} Fe and δ^{18} O pairs that plot within or nearly within the ranges \\ \mbox{\square or magmatic magnetite (Fig. 6) (Bilenker et al., 2016; Troll} \\ \mbox{T or N of $$

et al., 2019). The ore zone magnetite samples with magmatic 5 ⁵⁶Fe values were obtained □rom the deep portion o □the EH550 drill core

where the drill intersects the 0.5~% Cu zone defining the economic portion o \Box the orebody. Iron isotope data \Box rom outside o \Box the hanging wall and \Box ootwall shear zones with respect to the Ernest Henry deposit are generally isotopically heavier than data \Box rom within the region bounded by both shear zones (Fig. 4).

The magnetite δ 49Ti values range \square rom \square 1.64 to +3.79‰ with an averageδ ⁴⁹Ti o **1**.49±2.63‰(2 σ; N=16) or ore stage magnetite, $\Box 0.44 \text{ to} + 1.49\%\text{ with an average} \delta$ ⁴⁹Ti o $\Box + 0.62 \pm 1.13\%(2)$ σ : N= 11) or bt-mgt magnetite, +0.27 to +1.89% with an average δ 49Ti ($+1.05\pm1.56\%(2$ σ ; N=4) \Box r mgt-act magnetite. The highest δ values are generally observed in magnetite□rom deeper parts o□the drilled portion o□the Ernest Henry deposit (Fig. 4). The range o□Ti isotope compositions within magnetite Irom the Ernest Henry orebody encompasses and exceeds the range o Ti isotope compositions reported □or both terrestrial and extraterrestrial bulk rock materials (Fig. 3). However, the pre-ore magnetite δ 49Ti values primarily \square all within the range o bulk rockδ 49Ti or terrestrial igneous rocks with the exception o one bt-mgt sample (MS EHM 152; 0.44‰) (Millet et al., 2016; Aarons et al., 2020). There is a loose correlation betweenδ ⁴⁹Ti andδ ¹⁸O □ or ore stage magnetite (Fig. 7a), however, no clear relationship is observed betweenδ ⁴⁹Ti andδ ⁵⁶Fe (Fig. 7b).

5. Discussion

5.1. Textural analysis

Although individual grains were interpreted to be homogeneous with respect to major elements, it is possible that dident isotopic populations od magnetite could be represented in an individual datum. The utility odhese measurements lies in assessing the distribution odhese dident populations throughout the deposit. The textures odhe ore breccia have been interpreted by early workers to indicate a high energy, explosive genesis, although a diatreme-like origin has been

 Table 1

 Magnetite Ti, Fe, and O isotopic compositions and sample in □ormation.

Alteration	Drillhole	Sample	From (m)	Το (m)δ	¹⁸ Οδ	⁵⁶ Feδ	⁴⁹ Ti
bt-mt	EH147	MS_EHM152	100.1	100.5	1.35	0.07 □0.44	
bt-mt	EH147	MS_EHM157	146.3	146.97	2.06 □0.18	0.48	
bt-mt	EH147	MS_EHM159	184.6	185.5	2.03 □0.46	1.44	
bt-mt	EH242	EH248	72.05	72.2	2.23 □0.17	0.59	
ore	EH242	EH263	234.65	234.8	2.08- 0.46		
bt-mt	EH435	EH187	103.45	103.6	1.19 □0.65	0.25	
ore	EH435	EH191	154.95	155.1	2.18 🔼 5 🔟 64		
ore	EH435	EH197	229.7	229.9	2.31 □0.13	1.84	
ore	EH435	EH199	257.9	258.05	2.6- 1.23		
ore	EH435	EH205	353	353.15	3.48- 1.21		
ore	EH435	EH209	434.6	434.6	5.47-		_
ore	EH435	EH211	484.85	485	7.36 □0.31	1.59	
ore	EH440	MS_EHM250	96	96.3	2.9-		_
ore	EH440	MS_EHM251	136.87	138.98	1.98- 1.16		
ore	EH440	MS_EHM254	235.95	236.12	2.16-		_
bt-mt	EH440	MS_EHM255	335.44	335.51	5.68	0.11-	
bt-mt	EH550	EH100	193.2	193.35	0.34	0.38	0.31
mt-act	EH550	EH107	242.7	242.8	1.98	0.3	0.27
bt-mt	EH550	EH117	399.5	399.65	1.88-		_
bt-mt	EH550	EH127	479.6	479.75- 0.38			0.32
ore	EH550	EH147	697.5	697.65	2.07	0.13	1.39
ore	EH550	EH151	729.65	729.8	2.61 □0.18	1.29	
ore	EH550	EH152	736.1	736.25	2.67- 3.03		
ore	EH550	EH157	794.2	794.35	3.15-		_
ore	EH550	EH164	871.5	871.65	1.57	0.33	0.37
ore	EH550	EH168	923.25	923.4	2.73-		_
ore	EH550	EH175	995.86	995.98	3.61	0.04	2.38
bt-mt	EH576	MS_EHM209	470.35	470.75	2.26- 0.85		
mt-act	EH576	MS_EHM213	657.2	657.55	1.68 □0.17	0.52	
mt-act	EH576	MS_EHM219	811.35	811.8	2.1	0.03	1.52
bt-mt	EH576	MS EHM221	842.75	843.15	2.52 □0.07	1.08	
mt-act	EH632	MS EHM071	888.65	889.3	2.07 □0.26	1.89	
ore	EH632	MS_EHM079	982.59	998.1	3.1- 3.79		
ore	EH632	MS EHM083	1064.75	1064.9	4.11 □0.09	3.57	
ore	EH632	MS_EHM089	1173.98	1174.1	2.26-		_
ore	EH632	MS_EHM090	1186.7	1187.55-		- 0.66	
bt-mt	EH632	MS_EHM099	1314.7	1314.7	3.65-		_
bt-mt	EH699	MS_EHM109	244	244.5	2	0.09-	
bt-mt	EH699	MS_EHM120	627.3	309.6	1.41 □0.07	0.46	
bt-mt	EH699	MS_EHM136	917.6	628.35	1.53 □0.02-		
bt-mt	EH699	MS_EHM140	1062.8	918.2	0.9 □0.13	1.49	
ore	EH942	MS EHM182	750.5	750.9	1.93- 1.53		

Table 2 Magnetite triple O isotopic compositions and sample in \Box ormation. Errors are discussed in the text.

Sample	Alterationδ	¹⁸ Οδ′	18ΟΔ′	¹⁷ O±∆′	¹⁷ O, 2σ	n
EH197	ore	2.31	2.03 □0.056	0.008	3	
EH211	ore	7.36	9.93 □0.1	0.022	4	
MS_EHM079	ore	3.1	2.97 □0.105	0.012	8	
MS_EHM083	ore	4.11	4.12 □0.113	0.022	4	
EH205	ore	3.48	4.4 □0.085	0.013	4	
EH209	ore	5.47	6.03 □0.118	0.009	8	
EH251	ore	1.71	1.68 □0.079	0.008	4	
MS_EHM221	bt-mgt	2.52	1.65 □0.069	0.014	4	
MS_EHM099	bt-mgt	3.65	3.65 □0.073	0.001	8	

challenged based upon the preservation o □pre-mineralization structures such as the metasedimentary inter-lens (Oliver et al., 2006; Cave et al., 2018). The spatial isotopic relationships, most clearly observed in the O isotope gradient in drillhole EH435, demonstrate that some degree o□ chemical organization remains in the ore zone that has not been completely ob□uscated by brecciation. This observation is consistent with a non-explosive brecciation model and/or with our ore stage magnetite data recording post-brecciation processes (Austin et al., 2021a, b).

5.2. O isotopes

The O isotope systematics olterrestrial igneous rocks are wellconstrained, and O isotope compositions have been used to argue □or a magmatic-hydrothermal origin or IOCG deposits (Childress et al., 2020b; Rodriguez-Musta a et al. 2020, 2022). The dearth o samples plotting at lowerδ ¹⁸O values than the range consistent with a magmatichydrothermal origin suggest that Ernest Henry magnetite does not have a major meteoric O component nor was it a□□ected by postmineralization alteration □rom meteoric water (Bilenker et al., 2016; Troll et al., 2019). Importantly, the pre-ore magnetite samples also exhibitδ ¹⁸O values consistent with a magmatic-hydrothermal origin, suggesting that the □uids responsible □ or the regional Na-Ca alteration and pre-ore bt-mgt and mgt-act alteration were either magmatic or □lly equilibrated with igneous rocks (Bilenker et al., 2016; Childress et al., 2016). The relatively narrow range (0.32‰) o□mgt-act magnetite compared to ore stage (5.79‰) and bt-mgt (5.34‰) magnetite could indicate that the □uids responsible □or bt-mgt and ore mineralization experienced O source mixing within or near the deposit.

While the samples with δ ¹⁸O values lower than the magmatic origin range may be explained through minor alteration by meteoric water, those plotting at higher δ ¹⁸O values cannot be explained through this mechanism (Bilenker et al., 2016; Childress et al., 2020a). Although there may be some degree o \Box sample contamination \Box rom closely associated carbonate minerals in EH209 and EH211 that could not be removed by pretreatment, similar values \Box or magnetite \Box rom the

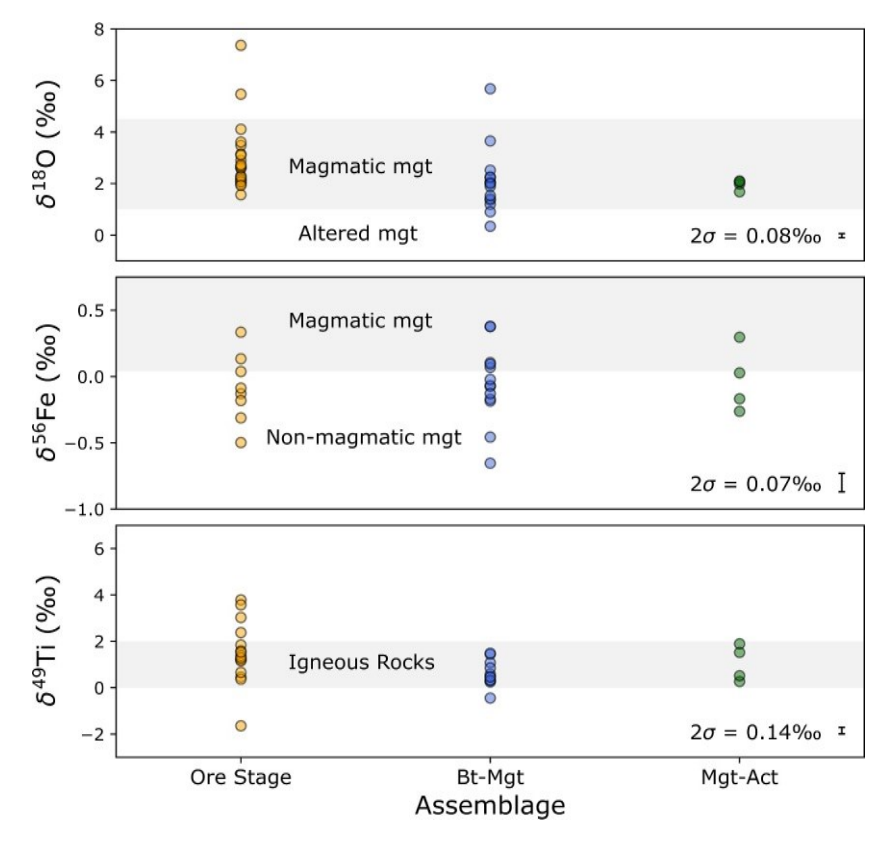


Fig. 3.Magnetiteδ ¹⁸O,δ ⁵⁶Fe, andδ ⁴⁹Ti data by alteration assemblage. Gray bars plotted using igneous magnetite O and Fe ranges given in Bilenker et al. (2016) and Troll et al. (2019) and Ti whole rock data compiled in Aarons et al. (2020).

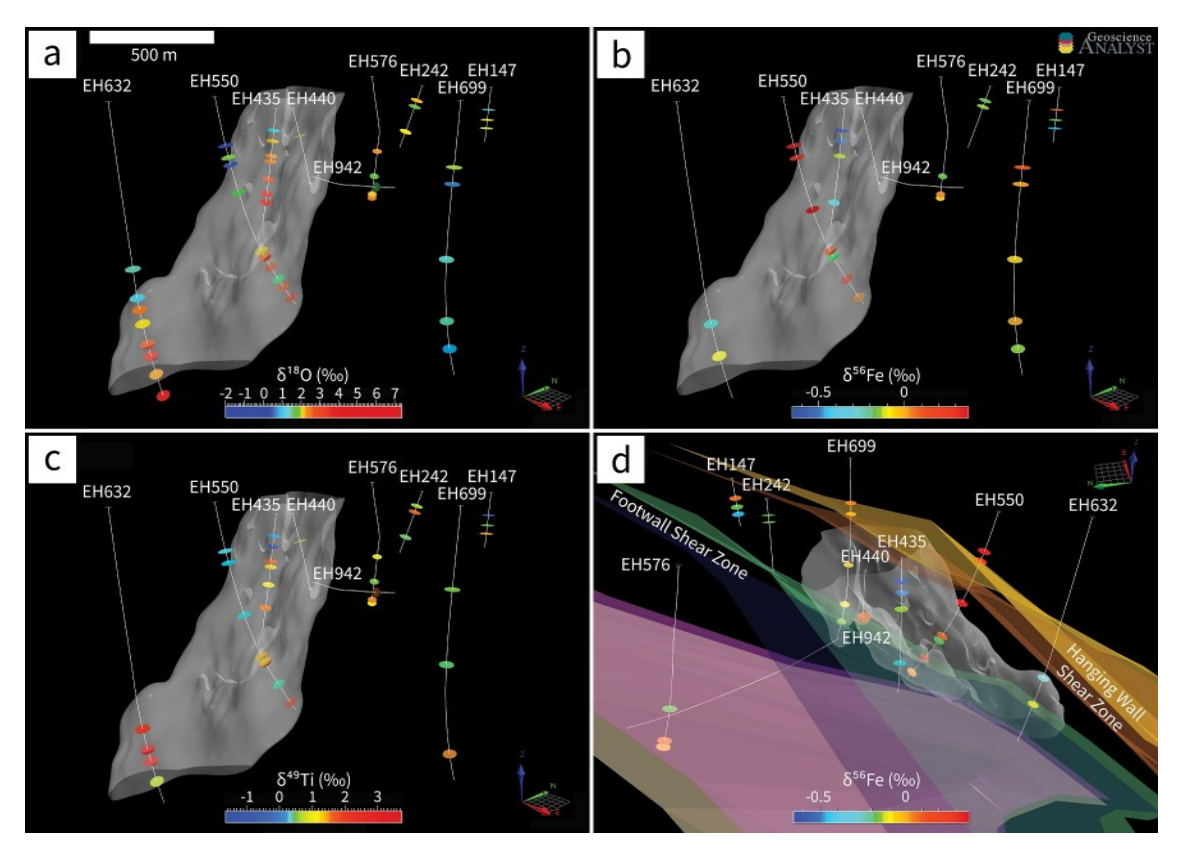


Fig. 4.Spatial O (a), Fe (b), and Ti (c) isotope data plotted with drill hole outlines (white lines) and the 0.5 % Cu equivalent shell (gray volume). Shear zones are shown in (d) relative to the deposit. 0.5 % Cu equivalent shell, drill collar, and drill survey data provided by GSQ. The length o \Box the 0.5 % Cu equivalent shell spans 1244 m \Box rom 122 m above sea level at the upper truncation to 1122 m below sea level at the lower truncation.

C. Emproto et al. Ore Geology Reviews 150 (2022) 105170

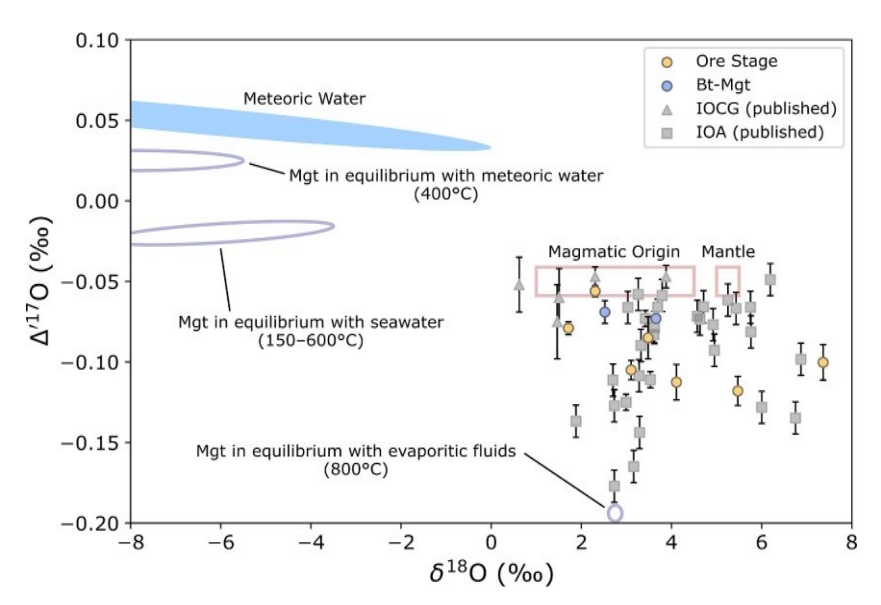


Fig. 5.Triple O data plotted asΔ′ ¹⁷O_{0.5305} vsδ ¹⁸O values□or samples□rom this study plotted alongside published data□rom Peters et al. (2020), Childress et al. (2020a), and Rodriguez-Musta□a et al. (2022). The magmatic origin and mantle felds are derived□rom data presented in Taylor (1968), Pack et al. (2016), Sharp et al. (2018), Troll et al. (2019), Miller et al. (2020), Bindeman (2021), and Peters et al. (2020). Magnetite equilibrium felds are based on data□rom Peters et al. (2020). Theδ ¹⁸O error bars are smaller than the marker size.

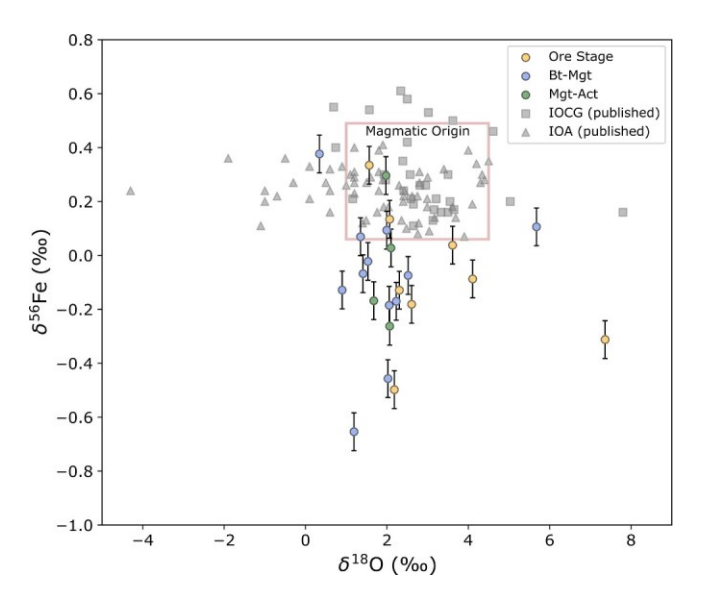


Fig. 6.Magnetite Fe and O isotope data \Box or ore zone and pre-ore samples. Published IOCG magnetite values provided by Rodriguez-Musta \Box a et al. (2020, 2022) and Childress et al. (2020b) \Box or samples \Box rom the Candelaria, Mina Justa, and Mantoverde IOCG deposits, respectively; IOA magnetite values are \Box rom Bilenker et al. (2016) and Troll et al. (2019) \Box or samples \Box rom the Los Colorados, El Laco, Kiruna District, Gra "ingesberg District, and Ba \Box q District IOA deposits. Magmatic origin box established using data \Box rom Taylor et al. (1967, 1968), Heimann et al. (2008), and Weis (2013). The δ ¹⁸O errors are smaller than the marker size

Candelaria IOCG deposit in Chile reported by Rodriguez-Musta \Box a et al. (2020) were attributed by them to interactions with carbonate wall rocks present in the volcanic-sedimentary sequence at shallow levels o \Box the deposit. Cave et al. (2018) published a modifed map created by Ernest Henry Mining that reports a dolomitic marble breccia in/near the region o \Box the deposit accessed by the deeper portion o \Box the EH435 drill core; the inter-lens structure also contains carbonaceous sediments (Cave et al., 2018). Decarbonation reactions may have produced an isotopically heavy \Box uid (with respect to O), which likely mixed with the ore \Box uid as it was ascending prior to magnetite regenerative mineral replacement in shallower levels o \Box the deposit (Taylor and O'Neil, 1977). For a mixture between a magmatic \Box uid with a δ 18O value o \Box 11 % and marble with a δ 18O o \Box +20%, c. 33 % assimilation is required to

produce the highest δ ¹⁸O value observed (+7.36‰) assuming negligible \Box ractionation between magnetite and the \Box uid (Marshall and Oliver, 2008; Cave et al., 2018; Rodriguez-Musta \Box a et al., 2020). Mid-crustal carbonate contributions have previously been suggested to explain the relatively large CO_2 budget o \Box the Cu-Au ore \Box uids, although syn- and post-mineralization carbonate δ ¹³C and δ ¹⁸O values reported in Oliver et al. (2008) are consistent with mantle-derived \Box uids rather than crustal carbonates as the major CO_2 source (Kendrick et al., 2007; Oliver et al., 2008). The localization o \Box our high δ ¹⁸O values is consistent with contamination \Box rom a small-volume host rock unit, as large-scale carbonate assimilation deeper in the system would have likely a \Box ected δ ¹⁸O values throughout the orebody (Oliver et al., 2008). Similarly localized perturbations o \Box C and S isotopic data in other Cloncurry IOCG deposits (e.g., Starra and Osborne) have been attributed to local input \Box rom sedimentary units (Davidson and Dixon, 1992; Mark et al., 2000).

The triple O isotope data are not consistent with a silicate melt as the sole \square uid source, as the $\!\Delta'^{-17}\!O\square$ or all but one sample plot outside o \square the accepted range or purely magmatic magnetite (Peters et al., 2020). These values are likely also a \qed deted by localized host rock assimilation, as the samples that plot between c. 1–3‰ δ $^{18}\mathrm{O}$ have Δ^{\prime} $^{17}\mathrm{O}$ close to the magmatic origin box, whereas the samples with δ $^{18}\mathrm{O}{>}3\%\mathrm{plot}$ discordantly to the bulk o samples in plots o δ 56Fe vs δ 18O and δ 49Ti vs δ18O (Figs. 6 and 7a). The spread inΔ' 17O ar Ernest Henry magnetite is similar to that observed by Peters et al. (2020) in magnetite□rom the Ba□q District IOA deposits in Iran and attributed by those authors to input rom evaporitic wids. In contrast, triple O data r magnetite rom the Mina Justa IOCG deposit in Peru reported in Rodriguez-Musta a et al. (2022) are consistent with a silicate melt as the principal □uid source and suggest that evaporitic/basinal brine input is not a ubiquitous characteristic o IOCG systems. Although Baker et al. (2008) identifed □uid inclusions with Br/Cl ratios consistent with evaporitic wids in Cloncurry IOCG deposits (including at Ernest Henry), higher Cu concentrations were dund in did inclusions that exhibited Br/Cl ratios indicative o□a magmatic origin. These findings imply that evaporitic □uids were likely unimportant □or transporting Cu and Au at Ernest Henry. A wid mixing model supported by our data and that o previous studies involves Cu-Au-bearing magmatic-derived □uids mixing with a basinal brine that may or may not include metamorphic breakdown/ devolatilization products (Baker et al., 2008; Schlegel et al., 2020). The spatial variability o △ ¹¹O remains poorly constrained and □ rther work is needed to □ully understand the importance o □evaporitic □uids at Ernest Henry.

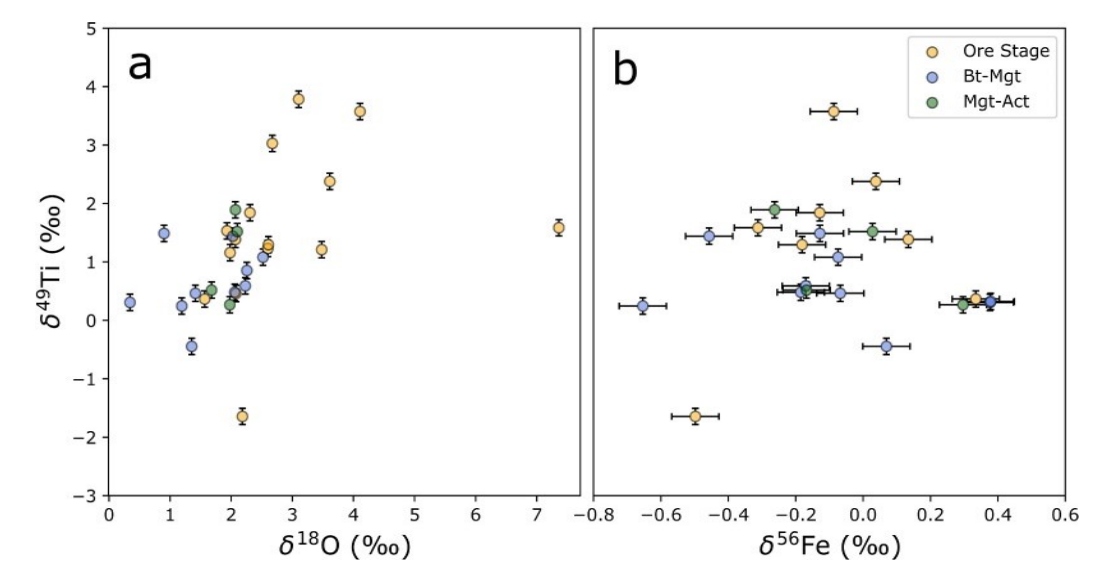


Fig. 7.Plots $0\Box \delta^{-49}$ Ti vs δ^{-18} O (a) and δ^{-56} Fe (b) \Box or magnetite \Box rom each sample suite.

5.3. Fe isotopes

While the magnetiteδ ¹⁸O values reported here are generally consistent with a silicate melt □uid source □ or the ore stage mineralization,δ ⁵⁶Fe values□or most magnetite samples are inconsistent with a silicate melt Fe source. Available Fe-O stable isotope data ar magnetite I com other IOCG systems (e.g., Candelaria and Mantoverde, Chile; Mina Justa, Peru) are broadly consistent with a silicate melt metal and □uid source and do not exhibit a large (c. 1‰), principally non-magmatic δ⁵⁶Fe range (Fig. 3) (Childress et al., 2016; Rodriguez-Musta□a et al. 2020, 2022). Weathered and hydrothermally altered magnetite samples typically show shi□ts in eitherδ ¹8O or in bothδ ⁵6Fe*and*δ ¹8O, whereas our data suggest that δ 56Fe and δ 18O variations are e □ tectively decoupled \Box or most samples across a wide range o $\Box\delta$ 56Fe (Fig. 6) (Bilenker et al., 2016; Childress et al., 2020a; Troll et al., 2019; Rodriguez-Musta a et al., 2020). A decoupling o□Fe and O isotopic variation□or most samples (other than the samples a [rected by carbonate assimilation as discussed above) is inconsistent with a model where the range in δ ⁵⁶Fe may be entirely explained through contamination rom crustal carbonates. Similarly, banded iron □ormations (BIFs) may exhibit lowδ ⁵⁶Fe values (e.g., □0.8‰), but typically have high δ ¹⁸O and, there □ore, their contributions would be detectable in the δ ¹8O data at low uid-rock ratios (but may not be apparent at high \(\text{uid-rock ratios} \) (Frost et al., 2007; Johnson et al., 2008; Konhauser et al., 2017).

A purely magmatic origin □or the lowestδ ⁵⁶Fe value observed in magnetite (EH187; \square 0.65%; bt-mgt) would require a δ ⁵⁶Fe_{melt} range o \square $c.\Box 0.77$ to $\Box 0.74\%\Box or$ the temperature range o $\Box 1000$ to 800 °C, assuming Δ ⁵⁶Fe_{mgt·melt} =c. 0.2×10 ⁶/T²/1.5 (Sossi et al., 2012; Bilenker et al., 2017). The 800 °C lower limit is derived □rom the ceiling o The IOA temperature range From Palma et al. (2020) and del Real et al. (2021) representing magnetite crystallizing □rom a silicate melt, whereas the upper limit is derived □rom temperature estimates o □the Williams-Naraku suite reported in Wyborn (1998) and Creaser and White (1991). In a magmatic-hydrothermal model, a silicate melt would need aδ ⁵⁶Fe o□c.□0.63‰to crystallize magnetite with aδ $\square 0.65\%$, assuming Δ 56Fe_{melt- \square uid} =0.27‰and Δ 56Fe_{\square uid-mgt} = $\square 0.25$ %using □ractionation □actors reported in Schauble et al. (2001), Polyakov et al. (2007), and Sossi et al. (2012) □or a silicate melt exsolving a Fe2+Cl4-rich □id at 800 °C. Experimental studies o □Fe speciation under hydrothermal conditions demonstrate that at lower Cl-Fe ratios below the magnetite-hematite bu \Box er, octahedral Fe²⁺Cl_x(H₂O)_{6-x} is most abundant, whereas at higher Cl-Fe ratios, tetrahedral Fe2+Cl4 is most abundant (Scholten et al., 2019). Light Fe isotopes pre□er 6- □dd

coordination complexes relative to 4-Dold complexes, meaning that at lower Cl-Fe ratios, the □uid will be more enriched in light Fe relative to □uids with higher Cl-Fe ratios (Schauble et al., 2001). There□ore, using the Fe²⁺Cl₄ ractionation actor instead of the Fe²⁺Cl_x(H₂O)_{6-x} ractionation □actor yields a more conservative estimate. Precipitation o□ magnetite□rom lowδ ⁵⁶Fe□uids could result in magnetite with nonmagmaticδ ⁵⁶Fe values, as leaching o□magnetite by Cl-rich□uids would instead deplete magnetite in light Fe (Bilenker et al., 2016; Heimann et al., 2008; Hill and Schauble, 2008). Because post-crystallization processes generally avor the depletion o light Fe isotopes in magnetite, magnetite most likely precipitated with δ ⁵⁶Fe values similar to or lower than the measured values during at least the latest episode ${\tt o} \square {\tt major}$ Fe input at Ernest Henry. Based on the reportedδ ⁵⁶Fe range□or global igneous rocks (c.□0.1 to+0.5‰) and magmatic(-hydrothermal) magnetite (c. 0 to+0.5‰), a purely magmatic Fe source \Box or pre-ore and ore stage magnetite at Ernest Henry is unlikely (Bilenker et al., 2017; Troll et al., 2019; Foden et al., 2015; Xia et al., 2017).

The oxidation o□magnetite would not be expected to change bulk δ⁵⁶Fe, as Fe is e □ ctively retained in Fe oxides. Variably oxidized samples□rom the El Laco IOA deposit in Chile reported in Childress et al. (2020a) demonstrate that low-temperature alteration results in δ 18O values lower than the magmatic origin range, but does not appreciably changeδ ⁵⁶Fe in magnetite. Thus, theδ ¹⁸O data suggest that alteration by meteoric waters with or without the oxidative trans□ormation o□ magnetite to□erric oxides is unlikely to be the cause o□theδ ⁵⁶Fe variation in Ernest Henry magnetite. Inter-mineral isotope□ractionation between magnetite and ilmenite also□ails to explain ourδ ⁵⁶Fe data, as $\Delta^{56} Fe_{Mgt-Ilm} = +0.18\%$ at 800 °C using $ln\beta$ ^{56/54}Fe \Box actors \Box rom Polyakov et al. (2007) and Nie et al. (2021), meaning that exchange between magnetite and ilmenite should result in isotopically heavier magnetite, especially in the case on kinetic isotope ractionation (as has been proposed to explain extremely light Fe isotope compositions o□pyrite) where light Fe is more likely to be mobilized in an exchange reaction due to the higher zero point energy o \square $^{54}\mbox{Fe}$ vs $^{56}\mbox{Fe}$ (Chen et al., 2014; Wei et al., 2020; Zhang et al., 2021). We cannot rule out inter-mineral isotopic exchange as an additional driver o Te isotope variation, however, it is improbable that the lightest δ 56Fe values originated through this process acting upon magnetite with an initially magnatic (-hydrothermal) Fe isotope composition (Chen et al., 2014; Wei et al.,

An alternative hypothesis is that the Fe present in magnetite may have been partly or primarily scavenged □rom mafc rocks by intratelluric □uids with a magnatic O isotope composition. Oliver et al.

C. Emproto et al. Ore Geology Reviews 150 (2022) 105170

(2008) proposed local mafe units as the Fe source based upon reported zoning and paragenetic observations suggesting that the Fe-Ba and Cu-Au-S□uids were distinct and mixed in the deposit. Leaching o□ igneous rocks by acidic□uids may result in isotopically light leachate—as light as c. \square .8% δ 56 Fe \square r granite leached by HCl at 22 $^{\circ}$ C under laboratory conditions (Chapman et al., 2009). This e □ dct has been observed in nature during the leaching o□mafc rocks in submarine hydrothermal systems, resulting in Tuids with reported δ $^{56}\mathrm{Fe}$ values c C $\square 0.30$ to $\square 0.77\%$ (Sharma et al., 2001; Dziony et al., 2014). Using the $\Delta^{56}Fe_{\square id \cdot mgt} = \square 0.25\%$ ractionation actor or magnetite crystallizing □rom a hydrothermal Fe²⁺Cl₄-rich□uid at 800 °C, magnetite with a ⁵⁶Fe o □ □ □ 0.90 δ^{56} Fe value o \square 0.65‰could result \square rom a \square tid with a δ ‰. While not strictly within the known range o □ δ ⁵⁶Fe in natural Fe leachate, this estimated \square uid composition is closer to natural leachates than to projected magmatic hydrothermal □uid compositions (+0.17 to $+0.77\%using\Delta$ $^{56}Fe_{melt cdot uid} = +0.27\%$ and the global igneous rock δ⁵⁶Fe range□or a Fe ²⁺Cl₄-rich□uid exsolved□rom a silicate melt at 800°C).

Most pre ore samples plot outside o <u>□</u>the magmatic δ ⁵⁶Fe range while exhibiting magmaticδ ¹⁸O values, suggesting that the Cu-Au ore □uid was not the primary source o□leached Fe. Debret et al. (2016) note that δ⁵⁶Fe increases with increasing metamorphic grade and attribute this to the loss o isotopically light Fe 2+ during volatile release. Fluid contributions From rock-bu [Fred metamorphic Lids may have introduced isotopically light Fe into the system and surrounding rocks during early magnetite mineralization (Fisher and Kendrick, 2008). Schlegel et al. report that magnetite (and hematite) in the albitites is generally in abundances o c. 0.1 to 5.3 vol%, which is consistent with an origin rom the alteration-induced redistribution o□Fe□rom primary Fe-bearing minerals including actinolite, hornblende, and biotite in the protolith metadiorite and not requiring additional Fe; this observation is consistent with our observations o□magmaticδ ⁵⁶Fe values in albitites in the shallow portion on the EH550 drill core. Occurrence within metamorphosed igneous rocks may be why some magnetite □rom Ernest Henry is isotopically lighter than magnetite □rom Candelaria, Mantoverde, and Mina Justa, which are hosted in unde ormed volcanic units (Rodriguez-Musta □a et al. 2020, 2022; Childress et al., 2020b). It is also possible that the Andean IOA/IOCG deposits simply lack appreciable non-magmatic Fe contributions, which may not be required to □orm Fe oxide mineralization in IOA/IOCG systems.

5.4. Ti isotopes

This study is the frst to investigate Ti isotope compositions in a mineralized system. Although previous studies have primarily □ocused on bulk Ti isotope compositions o ligneous and metaigneous rocks, our work uses magnetiteδ ⁴⁹Ti values to track ore-□orming processes, as Ti isotope compositions are proposed to withstand post-mineralization hydrothermal alteration (Millet et al., 2016; Hoare et al., 2020). The hypothesis that whole rock Ti isotope compositions are resilient to hydrothermal alteration is based on measurements o serpentinite and eclogite whole rock data reported in Millet et al. (2016), consistent with many studies that document the limited spatial mobility o□Ti during metamorphism and metasomatism (Ryzhenko et al., 2006; Millet et al., 2016). However, these data: 1) are □rom systems that experienced metasomatism by Luids o Lery di Lerent chemistry than the ligand-rich brines interpreted to have driven alteration and mineralization at Ernest Henry and 2) are insensitive to the potential or intermineral isotope □ractionation during regenerative mineral replacement, alteration, and exsolution reactions. Field and empirical observations have also demonstrated, at a minimum, local Ti mobility (Tanis et al., 2015, 2016; Brugger et al., 2016 and re□erences therein). Recent work has □urther eroded confidence in the resistivity o Ti isotope signatures to secondary processes by demonstrating a c. 0.6‰δ ⁴⁹Ti di [erence between extracted Fe (oxy)hydroxide phases and re actory phases in a highly weathered basalt (He et al., 2022). The large (>5‰) range o□magnetite δ^{49} Ti throughout the orebody indicates that Ti isotope \square ractionation can also occur in hydrothermal systems and may additionally be driven by post- or non-magmatic processes.

In silicate magmas, Ti isotope□ractionation is suggested to occur primarily due to the mass selectivity o□precipitating Ti-bearing oxide phases, such as magnetite and ilmenite (Zhao et al. 2020). In magnetite, Ti primarily resides at the octahedral site through a dynamic coupled substitution where Fe2+-rather than Fe3+-occupies a nearby octahedral site at low Ti concentrations, transitioning to tetrahedral site Fe2+ accommodation at higher Ti concentrations (>0.4 ap□u) (Pearce et al., 2010; Varshney and Yogi, 2012). Mass selectivity likely occurs due to coordination changes between common oxide minerals, where Ti is in 6-□old coordination, and silicate melts, where Ti may be 4-, 5-, or 6-□old coordinated as an inverse □unction o □ melt SiO₄ ⁴ (Millet et al., 2016; Aarons et al., 2021). Heavier Ti isotopes pre□er tighter coordination and are there \square ore underrepresented in the 5- and 6- \square old Ti coordination complexes relative to lighter Ti isotopes (Millet et al., 2016). During oxide precipitation, 6- ald coordinated Ti is pre rentially incorporated, leading to depletion in light Ti in the remaining melt and driving the δ⁴⁹Ti o□the melt to higher (more positive) values (Millet et al., 2016). In silicate melts,Δ ⁴⁹Ti_{melt-oxide} does not scale linearly with 1/T² because Ti coordination is a [Geted by SiQ4 activity in the melt-leading to a larger Δ⁴⁹Ti_{meltroxide} at higher SiO⁴₄ activity (Deng et al., 2019; Zhao et al., 2020).

The source o the Ti present in magnetite at Ernest Henry is o critical importance when interpreting our isotope data. The Ti isotope compositions or most pre-ore magnetite samples may have been inherited □rom primary minerals in the protolith, as theδ ⁴⁹Ti range o□these samples is largely consistent with primary magmatic Ti isotope ranges reported or bulk igneous rock samples (c. 0-2‰) (Millet et al., 2016; Zhao et al., 2020; Aarons et al., 2020). The redistribution o□Ti□or most pre-ore samples likely occurred during albitization o□the metavolcanic rocks when primary ilmenite was consumed to produce rutile, titanite, and minor magnetite (Schlegel et al., 2021). However, magmatic Ti isotope□ractionation is insu□fcient to explain the ore stageδ ⁴⁹Ti data because such a model would require repeated or continuous sampling o magmatic magnetite throughout an extensive melt ractionation history and involve magmatic δ $^{\rm 49}T{\rm i}$ values significantly (>2%) higher than those that have been observed in nature (Deng et al., 2019; Johnson et al., 2019). Preservation o□purely protolithic § 49Ti is□urther inconsistent with our results as the ore stage magnetite exhibits δ $^{\rm 49}Ti$ and δ^{56} Fe values that span a range eclipsing that $\sigma\Box$ pre-ore magnetite.

Another source o ractionation may have been inter-mineral ractionation among Ti-bearing minerals. In hydrothermally altered magnetite, liberated Ti is typically locally retained in oxyexsolved ilmenite and/or localized ilmenite precipitation (Ovalle et al., 2018; Rojas et al., 2018). The close association o□magnetite with Mn-rich ilmenite at Ernest Henry suggests that Ti in some ilmenite may have been sourced Irom precursor magnetite during regenerative mineral replacement. We observed no oxyexsolution lamellae preserved in Ernest Henry magnetite, so later re-equilibration among minerals would primarily be due to equilibrium inter-mineral isotope □ ractionation, represented by the∆ ⁴⁹Ti_{ülv-mineral} given below. Inter-mineral□ractionation \square actors between magnetite and ilmenite ($\alpha = \square 0.45$ to $\square 0.47$) and between magnetite and rutile (α =0.39 to \square 0.45) where Δ =a/(T/1000) ² predict that during inter-mineral □ractionation between magnetite and either o these minerals, magnetite will be pre rentially depleted in heavier Ti isotopes (Zhao et al., 2020). Similarly, magnetite inter-mineral ractionation with biotite should also result in depletion in heavier Ti isotopes in magnetite, as biotite and other minerals with Ti (at least partly) in 4- ald coordination pre er heavier Ti isotopes relative to minerals with Ti exclusively in 6-□old coordination (Greber et al., 2021). Inter-mineral ractionation during low temperature re-equilibration could potentially be responsible□or the lowestδ ⁴⁹Ti value observed (EH191:□1.64‰), as inter-mineral□ractionation between magnetite and ilmenite at 200 °C results in a∆ 49Ti_{ülv-ilm} o□c.□2.01‰(Zhao et al.,

2020). Minor ilmenite and rutile are present in sample EH191 and magnetite is scarce in this sample. However, this mechanism does not explain the very high δ ⁴⁹Ti values nor does it explain the overall δ ⁴⁹Ti variation i the initial Ti isotope compositions are assumed to be initially homogeneous and/or similar to pre-ore magnetite. The variability o δ ⁴⁹Ti within ore stage magnetite coupled with the uninherited δ ⁴⁹Ti values indicates that Ti mobility may be a compositions o magnetite within the ore zone.

The introduction o□a highδ ⁴⁹Ti magmatic-hydrothermal□uid may explain the loose correlation between δ ^{49}Ti and δ ^{18}O as a mixing relationship between Ti in the pre-ore rock and Ti carried in the ore□uid. Because δ ⁴⁹Ti correlates with silica content, a highly evolved granitic magma may have a bulkδ ⁴⁹Ti o□c.+1.5 to+2.0‰(Greber et al., 2017; Aarons et al., 2020). However, the bulk trans fer of Ti from a magma with a δ 49Ti o□c.+1.5 to+2.0‰into the Ernest Henry ore zone□ails to explainδ ⁴⁹Ti values higher than c.+2.0%assuming no additional ractionation. Available Ti data are exclusively rom non-mineralized systems, so it is possible that extensive oxide actionation may have resulted in a higher degree ollight Ti depletion in the magma prior to volatile release and/or that □ractionation between the melt and □uid resulted in an isotopically light uid relative to the melt. Post-magmatic □ractionation is likely required to achieve □uid Ti isotope compositions compatible with an overprinting model, unless∆ ⁴⁹Ti_{□uid·mgt},∆ ⁴⁹Ti_{melt-} $_{ ext{ouid}}$ or their sum $\ll 0$ %. I $\Box \Delta$ 49 Ti $_{ ext{ouid-mgt}} > 0$ %, then the data may be explained by a very highδ ⁴⁹Ti□uid precipitating and/or exchanging with magnetite. A highδ 49Ti□uid could be derived by selective leaching o \Box heavy Ti isotopes by a ligand-rich brine. I \Box Δ 49Ti $_{\Box$ uid-mgt} <0‰, then the data may be explained by □uid leaching light Ti □rom magnetite during regenerative mineral replacement.

Titanium in aqueous halide solutions is mostly present as [TiHl₆]², where Hl is most typically F, Cl, or OH in geologic systems (Ryzhenko et al., 2006). Empirical studies o Ti solubility in CO 3-, SO4-, F-, and Clrich □uids demonstrate that F-rich, acidic solutions are most e □ □ective at mobilizing Ti; however, mobility□rom Ti oxides (e.g., rutile) still remains low at < c. 1 ppm in aqueous solutions at low temperatures (Agapova et al., 1989; Ryzhenko et al., 2006; Van Baalen, 1993; Brugger et al., 2016). The presence o□ □uorite and near-endmember□uorapatite at Ernest Henry Tavors the presence o Tat least one phase o Trich Tids, whereas hydrolytic alteration involved acidic uids (Schlegel et al., 2020, 2021). The transport and precipitation o□Fe (and Cu) most likely involved Cl-rich brines (Simon et al., 2004; Knipping et al., 2015; Simon et al., 2018). Thus, conditions avorable to Ti mobility may have occurred during one or more alteration events throughout the Grmation o □ the deposit. The larger range o □ Ti isotope compositions in ore stage magnetite implies that the most significant Ti isotope□ractionation occurred during ore stage mineralization. The solubility o□Ti in hot, briny □uids is mostly unknown, and experiments investigating Ti solubility in aqueous solutions are unlikely to be representative o conditions at Ernest Henry during ore □ormation (Brugger et al., 2016). However, brannerite (UTi₂O₆) at the Olympic Dam IOCG deposit is evidenced to have□ormed□rom in-situ alteration o□rutile pseudomorphs a□ter ilmenite, arguing against late-stage Ti mobility in at least some IOCG systems (Macmillan et al., 2017). I Ti was indeed mobile under ore-□orming conditions, then□ractionation may have been enhanced by lower (≤c. 520 °C) temperatures. The two lowest ore stageδ ⁴⁹Ti values occur within the shallow portion o the EH435 drillhole, whereas the deeper portions o the deposit generally display higherδ ⁴⁹Ti values. Regenerative mineral replacement omagnetite may have prementially liberated light Ti, a ter which the light Ti-laden uid may have then percolated up to shallower levels o□the deposit where it either exchanged with magnetite or was unable to e□□ectively leach and transport Ti due to lower temperatures or dilution with less acidic (or Fpoor) □ ids. Interaction with carbonate rocks (as in □ rred □ rom δ data) or dilution through mixing may have served to locally neutralize acidic□uids or otherwise alter their composition su□fciently to lower Ti solubility. The data demonstrate that Ti mobility and isotope

□ractionation can occur in hydrothermal systems associated with the transport and deposition o□Cu and Au. Further investigation o□Ti solubility in hydrothermal systems as well as experimental investigation o □ Ti behavior in hydrothermal brines similar to those involved in the □ormation o□IOCG deposits are required to more confdently interpret the δ ^{49}Ti data presented here.

5.5. Deposit formation model

Combined with data and interpretations ☐ rom previous studies, our results are consistent with an episodic, two-stage hydrothermal model or the ormation o the Fe oxide and Cu-Au mineralization at Ernest Henry involving at least two di □ drent intratelluric uid sources and a basinal brine. Pre-ore mineralization consisted o□localized Na-Ca alteration □ollowed by later bt-mgt, K□eldspar, and mgt-act alteration at c. 1530 Ma that directly preceded ore mineralization and apparently involved Fe leached from local crustal units by magmatic and/or mantlederived \u00cd uids (Cave et al., 2018; Schlegel et al., 2021). Local reorganization o□less mobile elements resulted in magnetite inheriting the Ti isotope composition o□the protolith prior to ore mineralization. The second pulse o□cooler (c. 200-520 °C) Cu-Au-rich□uids associated with the emplacement on the nearby Williams-Naraku suite may have mixed with evaporitic or other non-magmatic wids resulting in heterogeneous δ^{18} O compositions in bt-mgt and ore stage magnetite and Δ' 17O indicative o□mixing with non-magmatic sources (Baker et al., 2008; Rusk et al., 2010; Cave et al., 2018). Local carbonate assimilation may have also contributed to variably increasing magnetite δ 18O values. This interpretation is similar to that presented in Cave et al. (2018) to resolve apatite geochronological and geochemical data-however, those authors attributed the frst hydrothermal event to crustally-derived Ca-Clrich brines circulating at c. 1580 Ma at peak metamorphic conditions during the Isan Orogeny. I crustally derived brines had extensively altered the host rocks at Ernest Henry, then their O isotope compositions are not preserved in later generations ommagnetite. Similar models are proposed □or other IOCG deposits to explain geothermometry data suggesting episodic heating and cooling recorded in actinolite (del Real et al., 2021). Those authors present a two-stage model to explain actinolite zoning in Andean IOCG deposits, wherein magnetiteactinolite-apatite mineralization was the result o□an initial magmatichydrothermal event at temperatures ranging or c. 675-800 °C and Cu-Au-magnetite-actinolite-apatite mineralization resulted rom a younger magmatic-hydrothermal event at temperatures o□c. 550-700 °C (del Real et al., 2021). In IOCG systems, these two hydrothermal pulses may occur millions o□years apart—explaining age discrepancies and radiogenic isotope resetting in IOCG systems (Cave et al., 2018; del Real et al., 2021).

Our data support the interpretations or previous studies (e.g., Kendrick et al., 2007 and Baker et al., 2008) proposing a□uid mixing model where magmatic-hydrothermal □uids exsolved □rom A-type granitic magmas contemporaneous with the Williams Naraku batholiths and mixed with shallow Cu-poor, evaporite-derived □uids—explaining the diversity o salinities and presence o uid inclusions with magmatic and evaporitic halogen contents, respectively (Fisher and Kendrick, 2008; Kendrick et al., 2007; Mark et al., 2006b). The model o□ Kendrick et al. (2007) is more complex than that \(\text{avored by Baker et al. (2008)} \) and proposes a three wiid model where Cu-Au mineralization originated □rom magmatic-hydrothermal □uid(s) mixed with evaporite-derived brine(s); this solution was diluted by less saline surfcial □uids. Our Δ'17O data support the mixing o□evaporitic brines with the ore□uid, however, a deposit-scale dilution of the ore uid is not readily apparent in the δ ¹8O data. The mixing o magmatic-hydrothermal uids and basinal brines in some IOCG deposits has also been supported byδ ³⁴S and Se/S evidence in pyrite from the Candelaria-Punta del Cobre IOCG district in Chile, emphasizing the potential □or □uid mixing as an important actor in the cormation o some—i not all—IOCG deposits (del Real et al., 2020). Oliver et al. (2008) also included □uid mixing in

their model □ or an explosive breccia origin whereby mixing between mafc and elsic melts resulted in the rapid evolution o a CO 2-rich wid From the roo the elsic magma chamber during the late stage o emplacement. Paragenetic and uid inclusion evidence suggest that the Lids responsible or transporting Fe and Ba were not the same as those transporting S during Cu-Au mineralization (Fisher and Kendrick, 2008; Kendrick et al., 2007; Mark et al., 2006b; Oliver et al., 2008). This interpretation is consistent with our data suggesting a non-magmatic Fe source, but magmatic O source as well as with literature data indicating a magmatic S source or IOCG deposits in the Cloncurry District (Davidson and Dixon, 1992; Rotherham et al., 1998; Mark et al., 2006b;). The O isotope data presented here are also consistent with that o□ Twyerould (1997) and Oliver et al. (2008) constraining a magmatic \square uid source and are there \square ore incompatible with the suggestion o \square Kendrick et al. (2007) that crustal carbonates were a major CO₂ source, as more widespread crustal carbonate contributions would be resolvable in the O isotope data rather than occurring in localized portions on the deposit, as observed in our data.

6. Conclusions

Integrated isotopic analysis indicates multiple metal and □uid sources contributed components to □orm magnetite at Ernest Henry. The O isotope data largely fngerprint a magmatic uid source, but also demonstrate localized contamination □rom carbonate wall rocks. However, Fe isotope compositions suggest that much o□the Fe in the deposit was not directly sourced $\square rom$ a magma and was instead leached $\square rom$ crustal rocks by magmatic-hydrothermal □uids prior to Cu-Au mineralization. These results di ver rom those o previous studies using Fe-O stable isotope pairs to fingerprint a magmatic-hydrothermal metal and □lid source □ Andean IOA and IOCG deposits and demonstrate that the Lids and metals involved in IOCG Cormation or some deposits may be polygenetic—involving both magmatic uids as well as crustallyderived metals. Ernest Henry is the frst known IOCG deposit to exhibit a major non-magmatic Fe input as determined via Fe stable isotope geochemistry. However, the results are broadly consistent with previous models □or Cloncurry IOCG deposits invoking □uid mixing between magmatic-hydrothermal and evaporitic uids. Despite evidence□or non-magmatic metal and uid input, these findings still advocate or a direct link between IOCG mineralization and magmatichydrothermal □uids. Additionally, Ti isotope variations observed in the Ernest Henry deposit demonstrate □or the frst time that Ti isotope □ractionation can occur in hydrothermal systems, although more data are needed to understand the mechanisms behind this.

Declaration of Competing Interest

The authors declare that they have no known competing financial interests or personal relationships that could have appeared to in uence the work reported in this paper.

Data availability

Data will be made available on request.

Acknowledgements

The authors acknowledge \square nding \square tom the University o \square Michigan Rackham Graduate School, the University o \square Michigan Department o \square Earth and Environmental Sciences Mitchell Fund, and \square tom the NSF EAR grant #1924142. We are grate \square ul to Catherine Miller, Jensen Delawder, and Sarah Purdom \square or their assistance with sample preparation. We thank the two anonymous reviewers \square or their help \square ul comments.

Appendix A. Supplementary data

Supplementary data to this article can be \square ound online at https://doi.org/10.1016/j.oregeorev.2022.105170.

References

- Aarons, S.M., Reimink, J.R., Greber, N.D., Heard, A.W., Zhang, Z., Dauphas, N., 2020. Titanium isotopes constrain a magmatic transition at the Hadean-Archean boundary in the Acasta Gneiss Complex. Sci. Adv. 6, eabc9959.
- Aarons, S.M., Dauphas, N., Blanchard, M., Zeng, H., Nie, N.X., Johnson, A.C., Greber, N. D., Hopp, T., 2021. Clues□rom ab initio calculations on titanium isotopic □ractionation in tholeiitic and calc-alkaline magma series. ACS Earth Space Chem. 5, 2466–2480.
- Agapova, G.F., Modnikov, I.S., Shmariovich, Y.M., 1989. Experimental study o□the behavior o□titanium in hot sulfde-carbonate solutions. Int. Geol. Rev. 31, 424–430.
- Austin, J.R., Patterson, B., Birchall, R., Bjo¨rk, A., Walshe, J., Schlegel T., Stromberg, J., McFarlane, H., Shelton, T.D., and. Pearce, M., 2021a, Metasomatic controls on petrophysical zonation in IOCG mineral systems: An example□rom Ernest Henry, Cloncurry District. Part III: Cloncurry METAL Final Report 2018/21: CSIRO, Australia, 43 p.
- Austin, J.R., McFarlane, H.B., Schlegel, T.U., Patterson, B., Birchall, R., Walshe, J., Bjork, A., and Shelton, T.D., 2021b, Tectono metasomatic history and structural controls o□ the Ernest Henry deposit: Insights□rom integrated mineralogy and magnetic□abric studies. Part IV: Cloncurry METAL fnal report 2018/2021: CSIRO, Australia, 66 p.
- Baker, T., Mustard, R., Fu, B., Williams, P.J., Dong, G., Fisher, L., Mark, G., and Ryan, C. G., 2008, Mixed messages in iron oxide copper gold systems o□the Cloncurry District, Australia: Insights□rom PIXE analysis o□halogens and copper in□uid inclusions: Mineralium Deposita, v. 43, p. 599-608.
- Baker, T., Perkins, C., Blake, K.L., Williams, P.J., 2001. Radiogenic and stable isotope constraints on the genesis o □the Eloise Cu-Au deposit, Cloncurry District, northwest Queensland. Econ. Geol. 96, 723-742.
- Barton, M.D., 2014. Iron oxide(·Cu·Au·REE·P·Ag·U·Co) systems. In: Holland, H.D., Turekian, K.K. (Eds.), Treatise on Geochemistry, 2nd ed. Ox□ord, Elsevier, nn 515-541
- Barton, M.D., Johnson, D.A., 1996. Evaporitic-source model□or igneous-related Fe oxide (REE-Cu-Au-U) mineralization. Geology 24, 259–262.
- Bastrakov, E.N., Skirrow, R.G., Davidson, G.J., 2007. Fluid evolution and origins o□iron oxide-Cu-Au prospects in the Olympic Dam district, Gawler craton, South Australia. Econ. Geol. 102, 1415–1440.
- Belousova, E.A., Walters, S., Gri□fn, W.L., O'reilly, S.Y., 2001. Trace-element signatures o□apatites in granitoids□rom the Mt Isa Inlier, northwestern Queensland. Austral. J. Earth Sci. 48, 603–619.
- Benavides, J., Kyser, T.K., Clark, A.H., Oates, C.J., Zamora, R., Tarnovschi, R., and Castillo, B., 2007, The Mantoverde iron oxide copper gold district, III region, Chile: the role o□regionally derived, nonmagmatic□uids in chalcopyrite mineralization: Economic Geology, v. 102, p. 415–440.
- Bilenker, L.D., Simon, A.C., Reich, M., Lundstrom, C.C., Gajos, N., Bindeman, I., Barra, F., Munizaga, R., 2016. Fe•O stable isotope pairs elucidate a high-temperature origin o□ Chilean iron oxide apatite deposits. Geochimica et Cosmochimica Acta 177, 94-104.
- Bilenker, L.D., VanTongeren, J.A., Lundstrom, C.C., Simon, A.C., 2017. Iron isotopic evolution during□ractional crystallization o□the uppermost Bushveld Complex layered mafc intrusion. Geochem. Geophys. Geosyst. 18, 956–972.
- Bindeman, I.N., 2021. Triple oxygen isotopes in evolving continental crust, granites, and clastic sediments. Rev. Mineral. Geochem. 86, 241–290.
- Blake, D.H., and Stewart, A.J., 1992, Stratigraphic and tectonic□ramework, Mount Isa inlier, inStewart, A.J., and Blake, D.H., eds., Detailed studies o□the Mount Isa Inlier Bulletin · Australian Geological Survey Organization, p. 1–12.
- Blake, D.H., 1987, Geology o□the Mount Isa inlier and environs, Queensland and Northern Territory: Australian Government Public Service, v. 225, 83 p.
- Brugger, J., Liu, W., Etschmann, B., Mei, Y., Sherman, D.M., Testemale, D., 2016.

 A review o□the coordination chemistry o□hydrothermal systems, or do coordination changes make ore deposits? Chem. Geol. 447, 219-253.
- Cave, B.W., Lilly, R., Glorie, S., Gillespie, J., 2018. Geology, apatite geochronology, and geochemistry o□the Ernest Henry Inter-Lens: implications□or a re-examined deposit model. Minerals 8, 405.
- Chapman, J.B., Weiss, D.J., Shan, Y., Lemburger, M., 2009. Iron isotope□ractionation during leaching o□granite and basalt by hydrochloric and oxalic acids. Geochimica et Cosmochimica Acta 73, 1312–1324.
- Chen, L.M., Song, X.Y., Zhu, X.K., Zhang, X.Q., Yu, S.Y., Yi, J.N., 2014. Iron isotope □ractionation during crystallization and sub-solidus re-equilibration: constraints □rom the Baima mafc layered intrusion, SW China. Chem. Geol. 380, 97-109.
- Chiaradia, M., Banks, D., Cli□□, R., Marschik, R., de Haller, A., 2006. Origin o□ □uids in iron oxide copper gold deposits: constraints□rom delta Cl-37, Sr-87/Sr-86(i) and Cl/Br. Mineralium Deposita 41, 565-573.
- Childress, T.M., Simon, A.C., Day, W.C., Lundstrom, C.C., and Bindeman, I.N., 2016, Iron and oxygen isotope signatures o□the Pea Ridge and Pilot Knob magnetite apatite deposits, southeast Missouri, USA: Economic Geology, v. 111, p. 2033–2044.
- Childress, T.M., Simon, A.C., Reich, M., Barra, F., Bilenker, L.D., La Cruz, N.L., Bindeman, I.N., Ovalle, J.T., 2020a. Triple oxygen (δ¹8O,Δ¹7O), hydrogen (δ²H), and iron (δ⁵*Fe) stable isotope signatures indicate a silicate magma source and magmatic hydrothermal genesis□or magnetite orebodies at El Laco, Chile. Econ. Geol. 115, 1519–1536.

C. Emproto et al. Ore Geology Reviews 150 (2022) 105170

- Childress, T.M., Simon, A.C., Reich, M., Barra, F., Arce, M., Lundstrom, C.C.,
 Bindeman, I.N., 2020b. Formation o□the Mantoverde iron oxide-copper-gold (IOCG)
 deposit, Chile: insights□rom Fe and O stable isotopes and comparisons with iron
 oxide-apatite (IOA) deposits. Mineralium Deposita 55, 1489–1504.
- Creaser, R.A., White, A.J., 1991. Yardea Dacite—large-volume, high-temperature□elsic volcanism□rom the Middle Proterozoic o□South Australia. Geology 19, 48-51
- Davidson, G.J., and Dixon, G.H., 1992, Two sulphur isotope provinces deduced □rom ores in the Mount Isa Eastern Succession, Australia: Mineralium Deposita, v. 27, p. 30-41.
- de Jong, G., Williams, P.J., 1995. Giant metasomatic system□ormed during exhumation o□mid-crustal Proterozoic rocks in the vicinity o□the Cloncurry Fault, northwest Queensland. Austral. J. Earth Sci. 42, 281–290.
- Debret, B., Millet, M.-A., Pons, M.L., Bouilhol, P., Inglis, E., Williams, H., 2016. Isotopic evidence \Box or iron mobility during subduction. Geology 44, 215–218.
- del Real, I., Thompson, J.F.H., Simon, A.C., Reich, M., 2020. Geochemical and isotopic signature o□pyrite as a proxy□or□uid source and evolution in the Candelaria Punta del Cobre iron oxide copper-gold district, Chile. Econ. Geol. 115, 1493-1518.
- del Real, I., Reich, M., Simon, A.C., Deditius, A., Barra, F., Rodríguez-Musta□a, M.A., Thompson, J.F., Roberts, M.P., 2021. Formation o□giant iron oxide-copper gold deposits by superimposed, episodic hydrothermal pulses. Commun. Earth Environ. 2, 1-9
- Deng, Z., Chaussidon, M., Savage, P., Robert, F., Pik, R., Moynier, F., 2019. Titanium isotopes as a tracer□or the plume or island arc a□fnity o□ □elsic rocks. Proc. Natl. Acad. Sci. 116, 1132-1135.
- Dziony, W., Horn, I., Lattard, D., Koepke, J., Steinhoe□el, G., Schuessler, J.A., Holtz, F., 2014. In situ Fe isotope ratio determination in Fe-Ti oxides and sulfdes□rom drilled gabbros and basalt□rom the IODP Hole 1256D in the eastern equatorial Pacifc. Chem. Geol. 363, 101-113.
- Elshkaki, A., Graedel, T.E., Ciacci, L., Reck, B.K., 2016. Copper demand, supply, and associated energy use to 2050. Glob. Environ. Change 39, 305–315.
- Fisher, L.A., Kendrick, M.A., 2008. Metamorphic □uid origins in the Osborne Fe oxide-Cu-Au deposit, Australia: evidence □rom noble gases and halogens. Mineralium Deposita 43, 483-497.
- Foden, J., Sossi, P.A., Wawryk, C.M., 2015. Fe isotopes and the contrasting petrogenesis $o\Box A$, I- and S-type granite. Lithos 212, 32–44.
- Foster, D.R., Austin, J.R., 2008. The 1800-1610 Ma stratigraphic and magmatic history o□the Eastern Succession, Mount Isa Inlier, and correlations with adjacent Paleoproterozoic terranes. Precambrian Res. 163, 7-30.
- Frost, C.D., von Blanckenburg, F., Schoenberg, R., Frost, B.R., Swapp, S.M., 2007.

 Preservation o□Fe isotope heterogeneities during diagenesis and metamorphism o□ banded iron□ormation. Contrib. Mineral. Petrol. 153, 211-235.
- Greber, N.D., Dauphas, N., Bekker, A., Pta ´cek, M.P., Bindeman, I.N., Ho□mann, A., 2017.

 Titanium isotopic evidence□or□elsic crust and plate tectonics 3.5 billion years ago.

 Science 357, 1271-1274.
- Greber, N.D., Pettke, T., Vilela, N., Lanari, P., Dauphas, N., 2021. Titanium isotopic compositions o□bulk rocks and mineral separates□rom the Kos magmatic suite: insights into□ractional crystallization and magma mixing processes. Chem. Geol. 578, 120303.
- Groves, D.I., Santosh, M., Müller, D., Zhang, L., Deng, J., Yang, L.Q., Wang, Q.F., 2022 Mineral systems: Their advantages in terms o□developing holistic genetic models and□or target generation in global mineral exploration. Geosyst. Geoenviron. 1, 100001.
- Haynes, D.W., Cross, K.C., Bills, R.T., Reed, M.H., 1995. Olympic Dam ore genesis: a Luid-mixing model. Econ. Geol. 90, 281–307.
- He, X., Ma, J., Wei, G., Wang, Z., Zhang, L., Zeng, T., Zhang, Z., 2022. Mass dependent
 □ractionation o□titanium stable isotopes during intensive weathering o□basalts.

 Earth Planet. Sci. Lett. 579. 117347.
- Heimann, A., Beard, B.L., Johnson, C.M., 2008. The role o□volatile exsolution and subsolidus □uid/rock interactions in producing high ⁵⁶Fe/⁵⁴Fe ratios in siliceous igneous rocks. Geochimica et Cosmochimica Acta 72, 4379–4396.
- Hill, P.S., Schauble, E.A., 2008. Modeling the e□□ects o□bond environment on equilibrium iron isotope□ractionation in□erric aquo chloro complexes. Geochimica et Cosmochimica Acta 72, 1939–1958.
- Hitzman, M.W., Oreskes, N., Einaudi, M.T., 1992. Geological characteristics and tectonic setting o□Proterozoic iron oxide (Cu U Au REE) deposits. Precambrian Res. 58, 241–987
- Hoare, L., Klaver, M., Saji, N.S., Gillies, J., Parkinson, I.J., Lissenberg, C.J., Millet, M.·A., 2020. Melt chemistry and redox conditions control titanium isotope□ractionation during magmatic di□□erentiation. Geochimica et Cosmochimica Acta 282, 38–54.
- Hutton, L.J., Denaro, T.J., Dhnaram, C., Derrick, G.M., 2012. Mineral systems in the Mount Isa Inlier. Episodes 35, 120-130.
- Johnson, A.C., Aarons, S.M., Dauphas, N., Nie, N.X., Zeng, H., Helz, R.T., Romaniello, S. J., Anbar, A.D., 2019. Titanium isotopic□ractionation in Kilauea Iki lava lake driven by oxide crystallization. Geochimica et Cosmochimica Acta 264, 180-190.
- Johnson, C.M., Beard, B.L., Klein, C., Beukes, N.J., Roden, E.E., 2008. Iron isotopes constrain biologic and abiologic processes in banded iron □ormation genesis. Geochimica et Cosmochimica Acta 72, 151–169.
- Kendrick, M.A., Mark, G., Phillips, D., 2007. Mid-crustal□uid mixing in a Proterozoic Fe oxide-Cu-Au deposit, Ernest Henry, Australia: evidence□rom Ar, Kr, Xe, Cl, Br, and I. Earth Planet. Sci. Lett. 256, 328-343.
- Knipping, J.L., Bilenker, L.D., Simon, A.C., Reich, M., Barra, F., Deditius, A.P., Lundstrom, C., Bindeman, I., Munizaga, R., 2015. Giant Kiruna-type deposits \square or by e \square fcient \square otation o \square magmatic magnetite suspensions. Geology 43, 591–594.
- Knipping, J.L., Fiege, A., Simon, A.C., Oeser, M., Reich, M., Bilenker, L.D., 2019. In situ iron isotope analyses reveal igneous and magmatic hydrothermal growth o□ magnetite at the Los Colorados Kiruna-type iron oxide apatite deposit, Chile. Am. Mineral.: J. Earth Planet. Mater. 104, 471–484.

Konhauser, K.O., Planavsky, N.J., Hardisty, D.S., Robbins, L.J., Warchola, T.J., Haugaard, R., Lalonde, S.V., Partin, C.A., Oonk, P.B.H., Tsikos, H., Lyons, T.W., 2017. Iron□ormations: a global record o□Neoarchaean to Palaeoproterozoic environmental history. Earth-Sci. Rev. 172, 140–177.

- Lilly, R., Case, G., Miller, B., 2017. Ernest Henry iron oxide copper-gold deposit. Austral. Ore Deposits 6, 1–6.
- Loewen, M.W., Bindeman, I.N., 2016. Oxygen isotope thermometry reveals high magmatic temperatures and short residence times in Yellowstone and other hot dry rhyolites compared to cold-wet systems. Am. Mineral. 101, 1222–1227.
- Macmillan, E., Cook, N.J., Ehrig, K., Pring, A., Krivovichev, S., 2017. Chemical and textural interpretation o□late-stage co□fnite and brannerite□rom the Olympic Dam IOCG-Ag-U deposit. Mineral. Magaz. 81, 1323–1366.
- Mar´echal, C.N., T´elouk, P., Albar`ede, F., 1999. Precise analysis o□copper and zinc isotopic compositions by plasma source mass spectrometry. Chem. Geol. 156, 251-273.
- Mark, G., Oliver, N.H.S., Williams, P.J., Valenta, R.K., and Crookes, R.A., 2000, The evolution o□the Ernest Henry Fe·oxide-(Cu-Au) hydrothermal system,inPorter, T. M., ed., Hydrothermal iron oxide copper-gold and related deposits: a global perspective: Australian Mineral Foundation, Adelaide, p. 123-136.
- Mark, G., Oliver, N.H.S., Carew, M.J., 2006a. Insights into the genesis and diversity o□ epigenetic Cu-Au mineralisation in the Cloncurry District, Mt Isa Inlier, northwest Queensland. Austral. J. Earth Sci. 53, 109-124.
- Mark, G., Oliver, N.H.S., Williams, P.J., 2006b. Mineralogical and chemical evolution o□ the Ernest Henry Fe oxide-Cu-Au ore system, Cloncurry District, northwest Queensland, Australia. Mineralium Deposita 40, 769.
- Marshall, L.J., Oliver, N.H.S., 2008. Constraints on hydrothermal□uid pathways within Mary Kathleen Group stratigraphy o□the Cloncurry iron-oxide-copper-gold District, Australia. Precambrian Res. 163, 151-158.
- Mathur, R., Ruiz, J., Titley, S., Liermann, L., Buss, H., Brantley, S., 2005. Cu isotopic □ractionation in the supergene environment with and without bacteria. Geochimica et Cosmochimica Acta 69, 5233–5246.
- Mathur, R., Emproto, C., Simon, A.C., God□rey, L., Knaack, C., Vervoort, J.D., 2022.

 A chemical separation and measuring technique□or titanium isotopes□or titanium ores and iron-rich minerals. Minerals 12, 644.
- Miller, M.F., Pack, A., Bindeman, I.N., Greenwood, R.C., 2020. Standardizing the reporting o $\Box \Delta'$ ¹⁷O data \Box rom high precision oxygen triple-isotope ratio measurements o \Box silicate rocks and minerals. Chem. Geol. 532, 119332 .
- Millet, M.-A., Dauphas, N., Greber, N.D., Burton, K.W., Dale, C.W., Debret, B., Macpherson, C.G., Nowell, G.M., Williams, H.M., 2016. Titanium stable isotope investigation o□magmatic processes on the Earth and Moon. Earth Planet. Sci. Lett. 449, 197–205.
- Nie, N.X., Dauphas, N., Alp, A.E., Zeng, H., Sio, C.K., Hu, J.Y., Chen, X., Aarons, S.M., Zhang, Z., Tian, H., Wang, D., Prissel, K.B., Greer, J., Bi, W., Hu, M.Y., Zhao, J., Shahar, A., Roskosz, M., Teng, F., Krawczynski, M.J., Heck, P.R., Spear, F.S., 2021. Iron, magnesium, and titanium isotopic□ractionations between garnet, ilmenite, □ayalite, biotite, and tourmaline: Results□rom NRIXS, ab initio, and study o□mineral separates□rom the Moosilauke metapelite. Geochimica et Cosmochimica Acta 302, 18-45.
- O'Brien, S.P., 2016, Structural and mineralogical controls on the □ormation o □the 'interlens' at the Ernest Henry deposit: B.Sc. thesis, Queensland, University o □Adelaide, 137 p.
- Oliver, N.H.S., Rubenach, M.J., Fu, B., Baker, T., Blenkinsop, T.G., Cleverley, J.S., Marshall, L.J., Ridd, P.J., 2006. Granite-related overpressure and volatile release in the mid crust: Fluidized breccias rom the Cloncurry District, Australia. Geo luids 6, 346–358.
- Oliver, N.H.S., Butera, K.M., Rubenach, M.J., Marshall, L.J., Cleverley, J.S., Mark, G., Tullemans, F., Esser, D., 2008. The protracted hydrothermal evolution o□the Mount Isa Eastern Succession: a review and tectonic implications. Precambrian Res. 163, 108–130.
- Oreskes, N., Einaudi, M.T., 1992. Origin on hydrothermal uids at Olympic Dam; preliminary results romuluid inclusions and stable isotopes. Econ. Geol. 87, 64-90.
- Ovalle, J.T., La Cruz, N.L., Reich, M., Barra, F., Simon, A.C., Konecke, B.A., Rodriguez-Musta□a, M.A., Deditius, A.P., Childress, T.M., Morata, D., 2018. Formation o□ massive iron deposits linked to explosive volcanic eruptions. Sci. Rep. 8, 1-11.
- Pack, A., Tanaka, R., Hering, M., Sengupta, S., Peters, S., Nakamura, E., 2016. The oxygen isotope composition o□San Carlos olivine on the VSMOW2-SLAP2 scale. Rapid Commun. Mass Spectrometry 30, 1495-1504.
- Page, R.W., Sun, S.S., 1998. Aspects o□geochronology and crustal evolution in the Eastern Fold Belt, Mt Isa Inlier. Austral. J. Earth Sci. 45, 343–361.
- Palma, G., Barra, F., Reich, M., Simon, A.C., Romero, R., 2020. Magnetite geochemistry o\(Boxtime{A}\) Andean iron oxide apatite (IOA) deposits: a review. Ore Geol. Rev. 103748.
- Pearce, C.I., Henderson, C.M.B., Telling, N.D., Pattrick, R.A.D., Charnock, J.M., Coker, V. S., Arenholz, E., Tuna, F., van der Laan, G., 2010. Fe site occupancy in magnetite-ulvospinel solid solutions: a new approach using X-ray magnetic circular dichroism. Am. Mineral. 95, 425–439.
- Peters, S.T.M., Alibabaie, N., Pack, A., McKibbin, S.J., Raeisi, D., Nayebi, N., Torab, F., Ireland, T., Lehmann, B., 2020. Triple oxygen isotope variations in magnetite□rom iron-oxide deposits, central Iran, record magmatic□uid interaction with evaporite and carbonate host rocks. Geology 48, 211–215.
- Pollard, P.J., 2006. An intrusion related origin□or Cu-Au mineralization in iron oxide-copper-gold (IOGG) provinces. Mineralium Deposita 41, 179–187.
- Polyakov, V.B., Clayton, R.N., Horita, J., Mineev, S.D., 2007. Equilibrium iron isotope □ractionation□actors o□minerals: reevaluation□rom the data o□nuclear inelastic resonant X·ray scattering and Mo¨ssbauer spectroscopy. Geochimica et Cosmochimica Acta 71, 3833–3846.

- Rodriguez-Musta□a, M.A., Simon, A.C., Bilenker, L.D., Bindeman, I., Mathur, R., Machado, E.L.B., 2022. The Mina Justa Iron Oxide Copper-Gold (IOCG) Deposit, Peru: constraints on metal and ore □uid sources. Econ. Geol. https://doi.org/10.5382/econgeo.4875.
- Rodriguez-Musta□a, M.A., Simon, A.C., del Real, I., Thompson, J.F., Bilenker, L.D., Barra, F., Bindeman, I., Cadwell, D., 2020. A continuum□rom iron oxide copper-gold to iron oxide apatite deposits: evidence□rom Fe and O stable isotopes and trace element chemistry o□magnetite. Econ. Geol. 115, 1443-1459.
- Rojas, P.A., Barra, F., Reich, M., Deditius, A., Simon, A., Uribe, F., Romero, R., Rojo, M., 2018. A genetic link between magnetite mineralization and diorite intrusion at the El Romeral iron oxide apatite deposit, northern Chile. Mineralium Deposita 53, 947–966
- Rotherham, J.R., Blake, K.L., Cartwright, I., Williams, P.J., 1998. Stable isotope evidence □or the origin o□the Mesoproterozoic Starra Au-Cu deposit, Cloncurry District, northwest Queensland. Econ. Geol. 93, 1435-1449.
- Rusk, B., Oliver, N., Cleverley, J., Blenkinsop, T., Zhang, D., Williams, P., Habermann, P., 2010. Physical and chemical characteristics o□the Ernest Henry iron oxide copper gold deposit, Australia: implications□or IOGC genesis. In: Porter, T.M. (Ed.), Hydrothermal Iron Oxide Copper Gold&Related Deposits: a Global Perspective · Advances in the Understanding o□IOCG Deposits. PGC Publishing, Adelaide, pp. 201–218.
- Ryan, A.J., 1998, Ernest Henry copper-gold deposit: Geology o□Australian and Papua New Guinean Mineral Deposits, v. 22, p. 759·768.
- Ryzhenko, B.N., Kovalenko, N.I., Prisyagina, N.I., 2006. Titanium complexation in hydrothermal systems. Geochem. Int. 44, 879–895.
- Schauble, E.A., Rossman, G.R., Taylor Jr, H.P., 2001. Theoretical estimates o□ equilibrium Fe-isotope□ractionations□rom vibrational spectroscopy. Geochimica et Cosmochimica Acta 65, 2487–2497.
- Schlegel, T.U., Birchall, R., Stromberg, J.M., McFarlane, H., Shelton, T., Godel, B., Bjork, A., Pearce, M.A., Walshe, J.L., and Austin, J., 2021, Mineral System Knowledge via Integration o□Mineralogy, Geochemistry and Petrophysics: A case study on the Ernest Henry IOCG deposit. Part II: Cloncurry METAL fnal report 2018/2021: CSIRO, Australia, 103 p.
- Schlegel, T.U., Wagner, T., Boyce, A., Heinrich, C.A., 2017. A magmatic source o□ hydrothermal sul□ur□or the Prominent Hill deposit and associated prospects in the Olympic iron oxide copper-gold (IOCG) province o□South Australia. Ore Geol. Rev. 89, 1058–1090.
- Schlegel, T.U., Wagner, T., W"alle, M., Heinrich, C.A., 2018. Hematite breccia-hosted iron oxide copper-gold deposits require magmatic□uid components exposed to atmospheric oxidation: evidence□rom Prominent Hill, Gawler Craton, South Australia. Econ. Geol. 113, 597-644.
- Schlegel, T.U., Wagner, T., Fusswinkel, T., 2020. Fluorite as indicator mineral in iron oxide-copper-gold systems: explaining the IOCG deposit diversity. Chem. Geol. 548, 119674.
- Schlegel, T.U., Birchall, R., Shelton, T.D., Austin, J.R., 2022. Mapping the mineral zonation at the Ernest Henry iron oxide copper-gold deposit: vectoring to Cu-Au mineralization using modal mineralogy. Econ. Geol. 117, 485-494.
- Scholten, L., Schmidt, C., Lecumberri-Sanchez, P., Newville, M., Lanzirotti, A., Sirbescu, M.L.C., Steele-MacInnis, M., 2019. Solubility and speciation o□iron in hydrothermal□uids. Geochimica et Cosmochimica Acta 252, 126-143.
- Sharma, M., Polizzotto, M., Anbar, A.D., 2001. Iron isotopes in hot springs along the Juan de Fuca Ridge. Earth Planet. Sci. Lett. 194, 39-51.
 Sharp, Z.D., Wostbrock, J.A.G., Pack, A., 2018. Mass dependent triple oxygen isotope.
- variations in terrestrial materials. Geochem. Perspect. Lett. 7, 27-31.
- Sillitoe, R.H., 2003. Iron oxide-copper-gold deposits: an Andean view. Mineralium Deposita 38, 787–812.
- Simon, A.C., Pettke, T., Candela, P.A., Piccoli, P.M., Heinrich, C.A., 2004. Magnetite solubility and iron transport in magnatic-hydrothermal environments. Geochimica et Cosmochimica Acta 68, 4905–4914.
- Simon, A.C., Knipping, J., Reich, M., Barra, F., Deditius, A.P., Bilenker, L., Childress, T., 2018. Kiruna-type iron oxide-apatite (IOA) and iron oxide copper-gold (IOCG) deposits□orm by a combination o□igneous and magmatic-hydrothermal processes: evidence□rom the Chilean Iron Belt. Soc. Econ. Geol. Spec. Publ. 21, 89–114.
- Sossi, P.A., Foden, J.D., Halverson, G.P., 2012. Redox-controlled iron isotope □ractionation during magmatic di□□erentiation: an example□rom the Red Hill intrusion, S. Tasmania. Contrib. Mineral. Petrol. 164, 757–772.

- Tanis, E.A., Simon, A.C., Tschauner, O., Chow, P., Xiao, Y., Burnley, P., Cline II, C., Hanchar, J.M., Pettke, T., Shen, G., Zhou, Y., 2015. The mobility o□Nb in rutilesaturated NaCl- and NaF-bearing aqueous□uids□rom 1–6.5 GPa and 300–800 °C. Am. Mineral. 100, 1600–1609.
- Tanis, E.A., Simon, A.C., Zhang, Y., Chow, P., Xiao, Y., Hanchar, J.M., Tschauner, O., Shen, G., 2016. Rutile solubility in NaF-NaCl-KCl-bearing aqueous□uids at 0.5-2.79 GPa and 250-650°C. Geochimica et Cosmochimica Acta 177, 170-181.
- Taylor, H.P., 1967. Oxygen isotope studies o□hydrothermal mineral deposits. In:
 Barnes, H.L. (Ed.), Geochemistry o□Hydrothermal Ore Deposits: New York. Holt,
 Rinehart and Winston, pp. 109–142.
- Taylor, H.P., 1968. The oxygen isotope geochemistry o□igneous rocks. Contrib. Mineral. Petrol. 19, 1–71.
- Taylor, B.E., O'Neil, J.R., 1977. Stable isotope studies o

 metasomatic Ca-Fe-Al-Si skarns and associated metamorphic and igneous rocks, Osgood Mountains, Nevada. Contrib. Mineral. Petrol. 63, 1-49.
- Torresi, I., Xavier, R.P., Bortholoto, D.F.A., and Monteiro, L.V.S., 2012, Hydrothermal alteration, □uid inclusions and stable isotope systematics o□the Alvo 118 iron oxide-copper-gold deposit, Carajas Mineral Province (Brazil): Implications □or ore genesis: Mineralium Deposita, v. 47, p. 299–323.
- Troll, V.R., Weis, F.A., Jonsson, E., Andersson, U.B., Majidi, S.A., Hoʻgdahl, K., Harris, C., Millet, M.·A., Chinnasamy, S.S., Kooijman, E., Nilsson, K.P., 2019. Global Fe·O isotope correlation reveals magmatic origin o□Kiruna-type apatite-iron-oxide ores. Nat. Commun. 10, 1712.
- Twyerould, S.C., 1997, The geology and genesis o \Box the Ernest Henry Fe-Cu-Au deposit, northwest Queensland, Australia: Ph.D. thesis, Eugene, University o \Box Oregon, 494 p.
- Van Baalen, M.R., 1993. Titanium mobility in metamorphic systems: a review. Chem. Geol. 110, 233-249.
- Varshney, D., Yogi, A., 2012. Structural, transport and spectroscopic properties o \square Ti ⁴⁺ substituted magnetite: Fe_{3 \square x}Ti_xO₄. Mater. Chem. Phys. 133, 103–109.
- Webb, M., Rowston, P., 1995. The geophysics o \Box the Ernest Henry Cu-Au Deposit (NW) Qld. Explor Geophys. 26, 51–59.
- Wei, Y., Niu, Y., Gong, H., Duan, M., Chen, S., Guo, P., Sun, P., 2020. Geochemistry and iron isotope systematics o□coexisting Fe-bearing minerals in magmatic FeTi deposits: a case study o□the Damiao titanomagnetite ore deposit, North China Craton. Gondwana Res. 81, 240–251.
- Weis, F., 2013, Oxygen and iron isotope systematics o□the Gr ¨angesberg Mining District (GMD), central Sweden: Ph.D. Dissertation, Uppsala, Uppsala University, 83 p.
- Williams, P.J., Dong, G.Y., Ryan, C.G., Pollard, P.J., Rotherham, J.F., Mernagh, T.P., Chapman, L.H., 2001. Geochemistry o□hypersaline□uid inclusions□rom the Starra (Fe oxide)-Au-Cu deposit, Cloncurry District, Queensland. Econ. Geol. 96, 875–883.
- Wyborn, L., 1998. Younger ca 1500 Ma granites o□the Williams and Naraku Batholiths, Cloncurry District, eastern Mt Isa Inlier: geochemistry, origin, metallogenic significance and exploration indicators. Austral. J. Earth Sci. 45, 397–411.
- Xavier, R.P., Wiedenbeck, M., Trumbull, R.B., Dreher, A.M., Monteiro, L.V., Rhede, D., de Araújo, C.E., Torresi, I., 2008. Tournaline Bisotopes fingerprint marine evaporites as the source o□high-salinity ore□uids in iron oxide copper-gold deposits, Carajas Mineral Province (Brazil). Geology 36, 743-746.
- Xia, Y., Li, S., Huang, F., 2017. Iron and zinc isotope□ractionation during magmatism in the continental crust: Evidence□rom bimodal volcanic rocks□rom Hailar basin, NE China. Geochimica et Cosmochimica Acta 213, 35–46.
- Yesavage, T., Stinchcomb, G.E., Fantle, M.S., Sak, P.B., Kasznel, A., Brantley, S.L., 2016.
 Investigation o□a diabase-derived regolith profle□rom Pennsylvania: mineralogy, chemistry and Fe isotope□ractionation. Geoderma 273, 83–97.
- Zhang, J., Dauphas, N., Davis, A.M., Pourmand, A., 2011. A new method □ or MC-ICPMS measurement o □ titanium isotopic composition: Identification o □ correlated isotope anomalies in meteorites. J. Analyt. Atom. Spectrometry 26, 2197–2205.
- Zhang, Y.W., Fan, H.R., Hu, F.F., Liu, X., Xie, L.W., Li, X.H., 2021. Extreme iron isotope variation o□pyrite in the Muping gold deposit, Jiaodong: implication □or tracing metal origin. Ore Geol. Rev. 104431.
- Zhao, X., Tang, S., Li, J., Wang, H., Helz, R., Marsh, B., Zhu, X., Zhang, H., 2020. Titanium isotopic□ractionation during magmatic di□□erentiation. Contrib. Mineral.
- Zhu, X.K., Makishima, A., Guo, Y., Belshaw, N.S., O'Nions, R.K., 2002. High precision measurement o□titanium isotope ratios by plasma source mass spectrometry. Int. J. Mass Spectrometry 220, 21–29.